Advances in Atmospheric Sciences
Impact Factor: 5.8
E-alert
ISSN 0256-1530
CN 11-1925/O4

Representation of the Stratospheric Circulation in CRA–40 Reanalysis: The Arctic Polar Vortex and the Quasi–Biennial Oscillation

Zixu WANG, Shirui YAN, Jinggao HU, Jiechun DENG, Rongcai REN, Jian RAO

Citation: Wang, Z. X., S. R. Yan, J. G. Hu, J. C. Deng, R. C. Ren, and J. Rao 2024: Representation of the Stratospheric Circulation in CRA–40 Reanalysis: The Arctic Polar Vortex and the Quasi–Biennial Oscillation, *Adv. Atmos. Sci.*, 41, 894–914. doi: 10.1007/s00376–023–3127–1.

View online: https://doi.org/10.1007/s00376–023–3127–1

ADVANCES IN ATMOSPHERIC SCIENCES, VOL. 41, MAY 2024, 894–914

• **Original Paper** •

Representation of the Stratospheric Circulation in CRA-40 Reanalysis: The Arctic Polar Vortex and the Quasi-Biennial Oscillation

Zixu WANG[1], Shirui YAN[2], Jinggao HU[*1], Jiechun DENG[1], Rongcai REN[3], and Jian RAO[1]

[1]*Key Laboratory of Meteorological Disaster, Ministry of Education (KLME), Joint International Research Laboratory of Climate and Environment Change (ILCEC), Collaborative Innovation Center on Forecast and Evaluation of Meteorological Disasters (CIC-FEMD), Nanjing University of Information Science & Technology, Nanjing* 210044, *China*

[2]*Key Laboratory for Semi-Arid Climate Change of the Ministry of Education, College of Atmospheric Sciences, Lanzhou University, Lanzhou* 730000, *China*

[3]*State Key Laboratory of Numerical Modeling for Atmospheric Sciences and Geophysical Fluid Dynamics, Institute of Atmospheric Physics, Chinese Academy of Sciences, Beijing* 100029, *China*

(Received 19 June 2023; revised 23 September 2023; accepted 13 October 2023)

ABSTRACT

The representation of the Arctic stratospheric circulation and the quasi-biennial oscillation (QBO) during the period 1981–2019 in a 40-yr Chinese global reanalysis dataset (CRA-40) is evaluated by comparing two widely used reanalysis datasets, ERA-5 and MERRA-2. CRA-40 demonstrates a comparable performance with ERA-5 and MERRA-2 in characterizing the winter and spring circulation in the lower and middle Arctic stratosphere. Specifically, differences in the climatological polar-mean temperature and polar night jet among the three reanalyses are within ±0.5 K and ±0.5 m s^{-1}, respectively. The onset dates of the stratospheric sudden warming and stratospheric final warming events at 10 hPa in CRA-40, together with the dynamics and circulation anomalies during the onset process of warming events, are nearly identical to the other two reanalyses with slight differences. By contrast, the CRA-40 dataset demonstrates a deteriorated performance in describing the QBO below 10 hPa compared to the other two reanalysis products, manifested by the larger easterly biases of the QBO index, the remarkably weaker amplitude of the QBO, and the weaker wavelet power of the QBO period. Such pronounced biases are mainly concentrated in the period 1981–98 and largely reduced by at least 39% in 1999–2019. Thus, particular caution is needed in studying the QBO based on CRA-40. All three reanalyses exhibit greater disagreement in the upper stratosphere compared to the lower and middle stratosphere for both the polar region and the tropics.

Key words: CRA-40, ERA-5, MERRA-2, Arctic stratosphere, the QBO

Citation: Wang, Z. X., S. R. Yan, J. G. Hu, J. C. Deng, R. C. Ren, and J. Rao, 2024: Representation of the stratospheric circulation in CRA-40 reanalysis: The Arctic polar vortex and the quasi-biennial oscillation. *Adv. Atmos. Sci.*, **41**(5), 894–914, https://doi.org/10.1007/s00376-023-3127-1.

Article Highlights:

- CRA-40 demonstrates an excellent performance in characterizing the winter and spring circulation in the lower and middle Arctic stratosphere.
- CRA-40 cannot well capture the characteristics of the quasi-biennial oscillation below 10 hPa.
- Considerable disagreement exists in the upper stratosphere in both the polar and tropical regions among CRA-40, ERA-5, and MERRA-2.

1. Introduction

The stratosphere, an atmospheric layer typically located 10–50 km above Earth's surface, can significantly impact tropospheric weather, climate, and human life (e.g., Andrews et al., 1987; Baldwin and Dunkerton, 2001; Baldwin et al., 2003). The circumpolar circulation in the stratosphere shows different characteristics in winter and summer. In the cold season, a strong polar vortex dominates the polar region, with strong westerlies along its edge. In contrast, an anticyclonic circulation controls the polar region during the warm season, and the circumpolar westerlies reverse to weak easterlies.

* Corresponding author: Jinggao HU
Email: jinggaohu@nuist.edu.cn

Stratospheric sudden warming (SSW) events represent major disruptions of the winter stratospheric polar vortex (Andrews et al., 1987; Charlton and Polvani, 2007; Baldwin et al., 2021, and references therein), which feature a rapid increase of temperature in the stratospheric polar regions over a short time. Strong SSWs (commonly designated as major SSWs; McInturff, 1978) can even reverse the direction of stratospheric zonal flow for several days. The frequency of major SSWs is about 0.6 yr^{-1} in the Northern Hemisphere (e.g., Limpasuvan et al., 2004; Charlton and Polvani, 2007). The dynamical influence of upward propagating planetary waves on the stratospheric mean flow causes the occurrence of SSWs (Matsuno, 1971). There is usually a similar warming in the polar stratosphere in spring, known as the stratospheric final warming (SFW) event (Andrews et al., 1987; Waugh et al., 1999; Black et al., 2006; Black and McDaniel, 2007a, b), which is one of the most important phenomena in the spring stratosphere. After its occurrence, the stratospheric circumpolar westerly wind completely reverses to an easterly wind, marking the arrival of the summer regime in the stratospheric polar region. The SFW onset is modulated by both vertically propagating planetary waves from the mid-and high-latitude troposphere to the stratosphere and the heating owing to solar radiation, therefore its timing exhibits an obvious interannual variability (e.g., Waugh and Rong, 2002; Black and McDaniel, 2007b). In the Northern Hemisphere, SFW usually occurs from mid-March to early May (Black et al., 2006; Wei et al., 2007; Ayarzagüena and Serrano, 2009; Li et al., 2012; Hu et al., 2014, 2018; Rao and Garfinkel, 2021).

In the lower and middle equatorial stratosphere, zonally symmetric westerly and easterly winds alternate around every two years. Since their period ranges from 24 to 30 months, with an average of about 28 months, this quasi-periodic variation in zonal winds is known as the quasi-biennial oscillation (QBO; Ebdon, 1960; Ebdon and Veryard, 1961; Reed et al., 1961; Angell and Korshover, 1964; Reed, 1964). The QBO is the largest source of interannual variability in the tropical stratosphere (e.g., Baldwin et al., 2001). It is forced by the interaction between the axisymmetric flow and a broad spectrum of waves dispersing upward from the troposphere (Lindzen and Holton, 1968; Holton and Lindzen, 1972; Dunkerton, 1997; Giorgetta et al., 2002). Although the SSW, SFW, and QBO are stratospheric phenomena, they can locally influence the stratospheric circulation or remotely impact the circulation in the lower mesosphere and weather and climate in the troposphere over the globe (e.g., Ren and Hu, 2014; Gray et al., 2018; Hu and Ren, 2018; Xie et al., 2018, 2020; Zhang et al., 2020; Baldwin et al., 2021; Rao et al., 2021; Wang et al., 2021; Cai et al., 2022; Hall et al., 2022; Huangfu et al., 2022).

Atmospheric reanalysis datasets provide a wide range of atmospheric variables in a standard format, extensively meeting the scientific community's demand for data. They have been widely used in atmospheric studies, especially in the stratosphere where observations are relatively sparse compared to the troposphere. Almost every set of atmospheric reanalysis has been evaluated to some extent regarding the representation of stratospheric atmospheric phenomena (e.g., Pawson and Fiorino, 1998, 1999; Randel et al., 2004; Manney et al., 2005a; Simmons et al., 2014; Kawatani et al., 2016; Long et al., 2017; Wright and Hindley, 2018; Essa et al., 2022). Stratosphere-troposphere Processes And their Role in Climate (SPARC) has also initiated a specialized project (i.e., the SPARC Reanalysis Intercomparison Project) to intercompare all major atmospheric reanalysis products (Fujiwara et al., 2017). Several outcomes can be summarized from previous studies. It is found that more recent reanalyses outperform their earlier versions in many aspects. For example, more recent reanalyses show fewer discontinuities in the temporal evolution of air temperature and wind (e.g., Long et al., 2017). ERA-5, the most recent global reanalysis, is argued to minimize the temperature bias from 30 to 70 hPa relative to the homogenized upper-air radiosonde observations (Essa et al., 2022). In addition, different reanalyses show strong agreement in the lower and middle stratosphere but feature large differences in the upper stratosphere due to fewer conventional observations available for assimilation (e.g., Kawatani et al., 2016; Long et al., 2017; Wright and Hindley, 2018; Essa et al., 2022). Even the earlier generation of reanalyses, such as ERA-40 and NCEP-1, can well characterize the lower stratospheric circulation in both polar regions and tropics (e.g., Manney et al., 2005b; Charlton and Polvani, 2007; Martineau and Son, 2010). Compared to the extratropical stratosphere, the representation of temperature and circulation in the tropical stratosphere exhibits a larger disagreement among the reanalyses (e.g., Long et al., 2017; Wright and Hindley, 2018; Essa et al., 2022).

Recently, the National Meteorological Information Center (NMIC) of the China Meteorological Administration (CMA) released a 40-yr global Chinese reanalysis (CRA-40) dataset (Liu et al., 2017; Zhao et al., 2019; Liang et al., 2020). The applicability of this dataset has been evaluated in various respects. Shen et al. (2022) analyzed the near-surface wind speed over China based on CRA-40, compared with four other global reanalysis products (ERA-5, NCEP-1, NCEP-2, and JRA-55). They pointed out that CRA-40 provides a more significant and closer correlation with the observations. Yang et al. (2021) concluded that CRA-40 outperformed the ERA-Interim dataset in terms of temperature change over the Tibetan Plateau. Zhao et al. (2021) verified the reliability of CRA-40 in characterizing the hydrological cycle over East China.

However, the previous assessments of the CRA-40 reanalysis focus on the meteorological elements on the land surface and in the troposphere. There has yet to be a study that compares the performance of CRA-40 in characterizing the stratospheric circulation with existing reanalysis products. The primary purpose of this study is to assess the capability and applicability of CRA-40 in representing the stratospheric circulation. We focus on the Arctic stratospheric circulation in

winter and spring and the QBO in the equatorial stratosphere.

The remainder of this paper is as follows. Section 2 describes the data and methods used. Section 3 then assesses the performance of CRA-40 in representing the Arctic stratospheric circulation. Section 4 examines the amplitude, period, and long-term trend of the QBO in CRA-40. Finally, section 5 provides a summary and conclusions.

2. Data and methods

The CMA started the reanalysis project in 2014 (Liu et al., 2017; Zhao et al., 2019). CRA-40 is the first-generation global atmosphere and land surface reanalysis dataset released by the CMA. The atmospheric model in the CRA Reanalysis system has a horizontal resolution of T574 (~34 km) with 64 hybrid σ–pressure layers in the vertical direction and a model top of 0.27 hPa (~55 km). The data is produced using 3D-Var assimilation. Further details on the dataset can be found in Liu et al. (2023). CRA-40 has been available from 1979 to the present.

We also use the ERA-5 and MERRA-2 reanalysis datasets for comparisons with CRA-40. ERA-5 is the fifth and latest generation of ECMWF atmospheric reanalysis of the global climate covering the period from 1940 to the present. It is produced using 4D-Var assimilation with a horizontal resolution of TL639 (~31 km), and it has 137 hybrid levels in the vertical with a model top at 0.01 hPa (~80 km). MERRA-2 is a global atmospheric reanalysis developed by NASA's GMAO covering the period from 1980 to the present. It is based on the GEOS 5.12.4 assimilation system, which uses a 3D-Var assimilation with an incremental analysis update. It has a horizontal resolution of 0.5° × 0.625° (latitude × longitude) grid and 72 hybrid levels in the vertical with a model top at 0.01 hPa (~80 km). Further details on the dataset can be found in Hersbach et al. (2020) for ERA-5 and Gelaro et al. (2017) for MERRA-2.

In this study, all the reanalysis datasets are horizontally interpolated onto a 1° × 1° (latitude × longitude) grid using the bilinear interpolation method for 17 pressure levels (925, 850, 700, 600, 500, 400, 300, 250, 200, 150, 100, 70, 50, 30, 20, 10, and 5 hPa). We limit our attention to CRA-40's performance in the lower (100, 70, and 50 hPa) and middle (30, 20, and 10 hPa) stratosphere due to the high disagreement in the upper stratosphere among major current reanalysis products. However, we retain a specific pressure level of the upper stratosphere (5 hPa) to facilitate the comparisons. We use data for the period spanning December 1980 to December 2019.

Major SSWs and SFWs are identified in these three reanalyses. Following Charlton and Polvani (2007), a major SSW event is identified when the zonal-mean westerly wind at 60°N and 10 hPa reverses to an easterly wind during the period from November to March. The onset date of a major SSW is defined as the first day when the zonal-mean westerly wind drops below zero. Following Black et al. (2006) and Hu et al. (2014), the SFW onset date is defined as the final date when the zonal-mean zonal wind in 60°–70°N at 10 hPa reverses to an easterly wind and never recovers until the subsequent autumn. If the reversed easterly wind returns to low values of westerly wind after the breakdown of the stratospheric polar vortex, the speed of returned westerly wind should be no more than 5 m s^{-1} and its duration cannot exceed 5 days. It is worth stating that a 20-day interval of the onset date must exist between two consecutive major SSWs and between a major SSW and SFW event (Charlton and Polvani, 2007). For brevity, we omit the word major in the following sections.

The Eliassen-Palm (EP) flux is employed to characterize the planetary wave activities during the occurrence of stratospheric warming events. Under the quasi-geostrophic approximation, the horizontal and vertical components of the EP flux can be expressed as follows (Andrews et al., 1987; McDaniel and Black, 2005):

$$F_\varphi = a\cos\varphi e^{-\frac{z}{H}}\left(-\overline{v'u'}\right), \tag{1}$$

$$F_z = af\cos\varphi e^{-\frac{z}{H}}\overline{v'\theta'}\left(\frac{\partial\overline{\theta}}{\partial z}\right)^{-1}, \tag{2}$$

where a is the radius of the earth, φ is the latitude, z is a log pressure coordinate with the scale height H, f is the Coriolis parameter, u and v represent the zonal wind and meridional wind, respectively, θ is the potential temperature, and F_φ and F_z are the horizontal and vertical components of the EP flux, respectively. The overbar and the prime denote the zonal mean and the zonal deviation from it, respectively.

In this study, we calculate the QBO amplitude using a method similar to Kawatani and Hamilton (2013). The monthly QBO index is defined as the zonal-mean zonal wind averaged over 10°S–10°N, which is then deseasonalized by subtracting the seasonal cycle averaged over 1981–2019 and smoothed by a 5-month running mean. Afterward, we calculate the monthly standard deviation of the resultant QBO index using a 96-month sliding window. Finally, the QBO amplitude is defined as the monthly standard deviation multiplied by $\sqrt{2}$, which is then averaged from January to December in each year to obtain the annual QBO amplitude.

In this paper, the spring, summer, autumn, and winter seasons are respectively defined by the months from March to May, from June to August, from September to November, and from December to February.

3. Characteristics of the Arctic stratosphere in CRA-40

3.1. *Climatology*

We first evaluate the performance of CRA-40 in characterizing the Arctic stratospheric polar vortex, focusing on the winter and spring seasons. Figure 1 shows the difference in the climatological winter-mean temperature at different stratospheric pressure levels between each pair of the three

reanalyses. The differences between ERA-5 and MERRA-2 in the lower and middle Arctic stratosphere are relatively small within ±0.5 K (Figs. 1f, i, l, o), while the differences between CRA-40 and the other two reanalyses are also not obvious at 50 and 30 hPa (Figs. 1j, k, m, n). These differences have increased in the polar region between 10 and 20 hPa but with small magnitudes (Figs. 1d, e, g, h). Overall, CRA-40 performs well in representing the climatological winter-mean temperature in the lower and middle Arctic stratosphere, although with a minor cold bias of 0 to –0.8 K.

However, compared with the middle and lower stratosphere, the differences among the three reanalyses in the upper stratosphere are remarkably enlarged (Figs. 1a–c), indicating considerable disagreement in characterizing the upper stratospheric circulation in the current reanalyses. In addition, in the lower tropical stratosphere, the differences

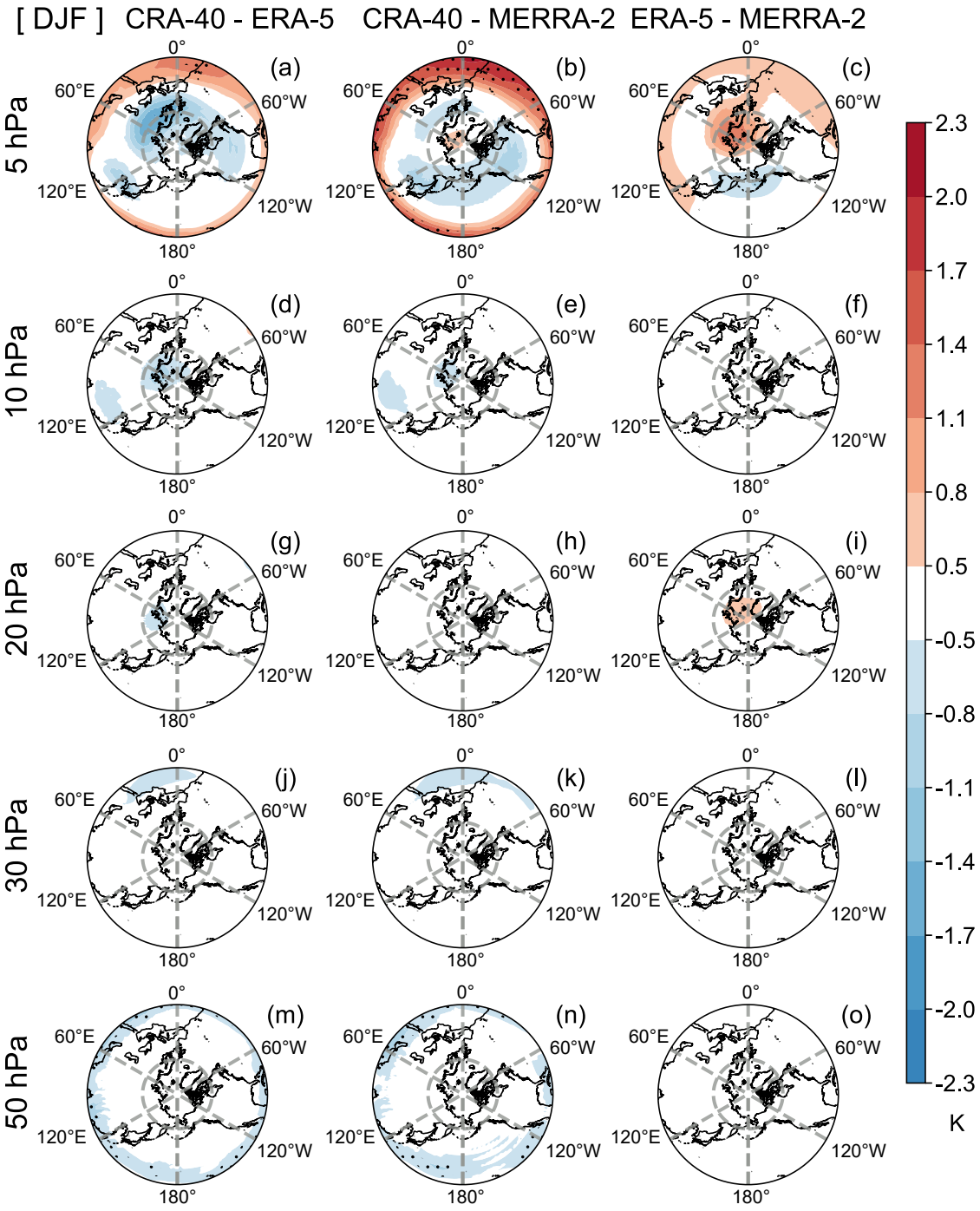

Fig. 1. The difference in climatological winter temperature at 5, 10, 20, 30, and 50 hPa during 1981–2019 (left panels) between CRA-40 and ERA-5, (middle panels) between CRA-40 and MERRA-2, and (right panels) between ERA-5 and MERRA-2, respectively.

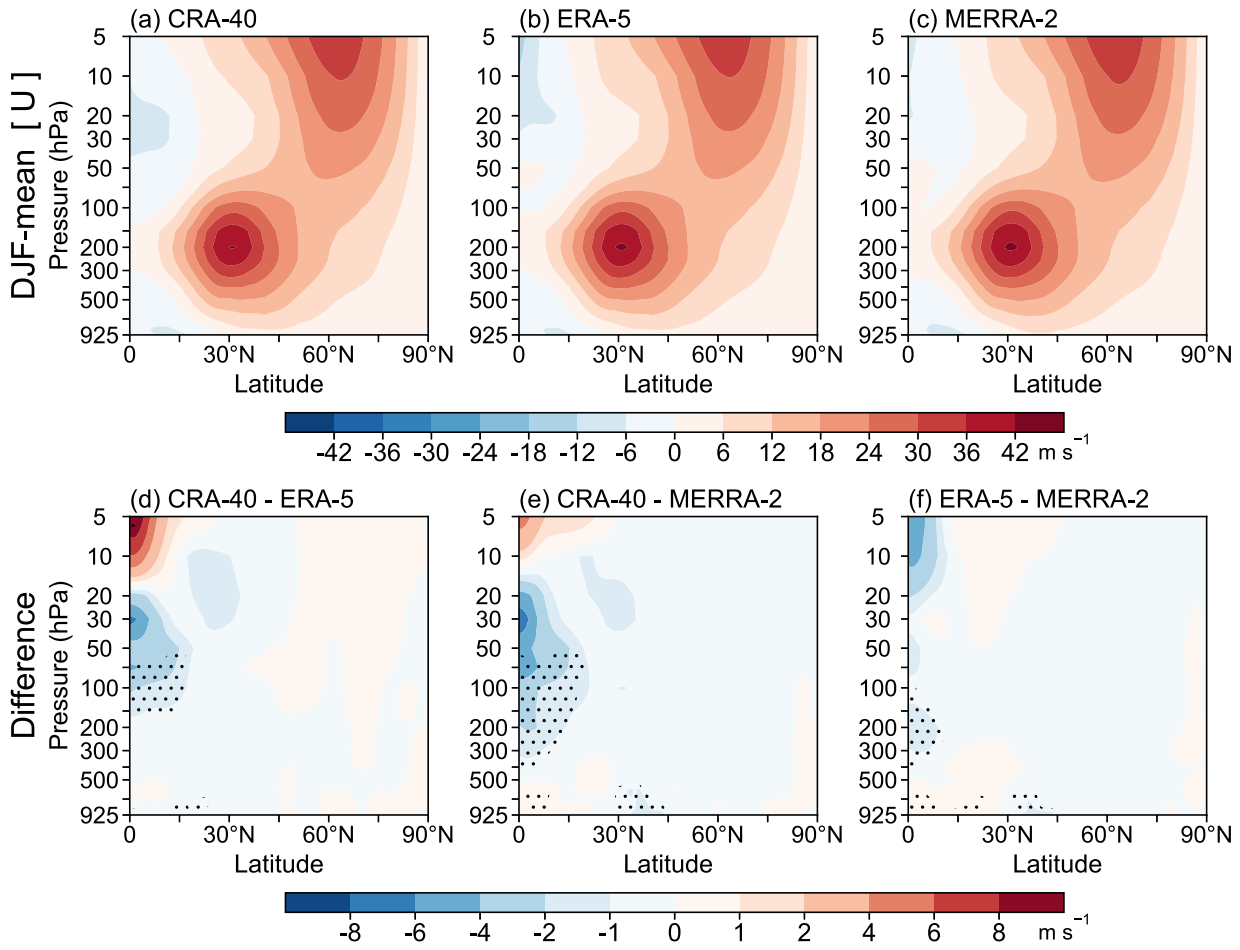

Fig. 2. (a–c) Latitude–height cross section of climatological zonal-mean zonal wind in winter during 1981–2019 in (a) CRA-40, (b) ERA-5, and (c) MERRA-2. (d–f) As in (a–c), but for the difference (d) between CRA-40 and ERA-5, (e) between CRA-40 and MERRA-2, and (f) between ERA-5 and MERRA-2, respectively. The dotted areas indicate the 95% confidence level for the differences.

between CRA-40 and the other two reanalyses are significant (Figs. 1m, n), which does not exist in those between ERA-5 and MERRA-2 (Fig. 1o). This indicates that CRA-40 may have pronounced biases in representing the winter QBO as compared to the other two reanalyses. The above findings can also be observed in the March-April season (Fig. S1 in the electronic supplementary material, ESM).

Figure 2 shows the latitude–height cross-section of the climatological zonal-mean zonal wind in winter in the three reanalyses and their differences. CRA-40 well describes the stratospheric polar night jet in the Arctic (Fig. 2a) with the differences from the other two reanalyses within ±1 m s^{-1} (Figs. 2d, e). Just as with the temperature, sizable differences in the zonal wind also exist in the tropics. CRA-40 has significant negative biases relative to ERA-5 and MERRA-2 in the upper troposphere and lower stratosphere, mainly from 200 to 50 hPa. By contrast, significant differences between ERA-5 and MERRA-2 can only be found in the tropical troposphere below 100 hPa. Again, this indicates that the description of the QBO in the lower stratosphere by CRA-40 may not be accurate enough. Similar results can be found in the March-April season (Fig. S2 in the ESM).

To further demonstrate the characterization of the Arctic stratospheric polar vortex, Figure 3 shows the daily evolution of the climatological zonal-mean zonal wind averaged in the core latitudes (60°–70°N) of the polar night jet with the differences among the three reanalyses. CRA-40 agrees well with the other two reanalyses regarding the climatological seasonal transition date when the westerly wind reverses to an easterly wind (Figs. 3a, c, e). The intensity of the polar night jet below 10 hPa in CRA-40 and ERA-5 is weaker than in MERRA-2, whereas the differences are relatively small (within ±0.5 m s^{-1}, Figs. 3d, f). The differences among the three reanalyses increase at 10 and 5 hPa, with the biases exceeding –1 m s^{-1} from late April to May between CRA-40 and ERA-5 and from late December to early January between ERA-5 and MERRA-2 (Figs. 3b, f).

3.2. *Monthly, interannual, and interdecadal variations*

3.2.1. *Monthly difference from November to April*

Figure 4 shows the monthly difference of zonal-mean

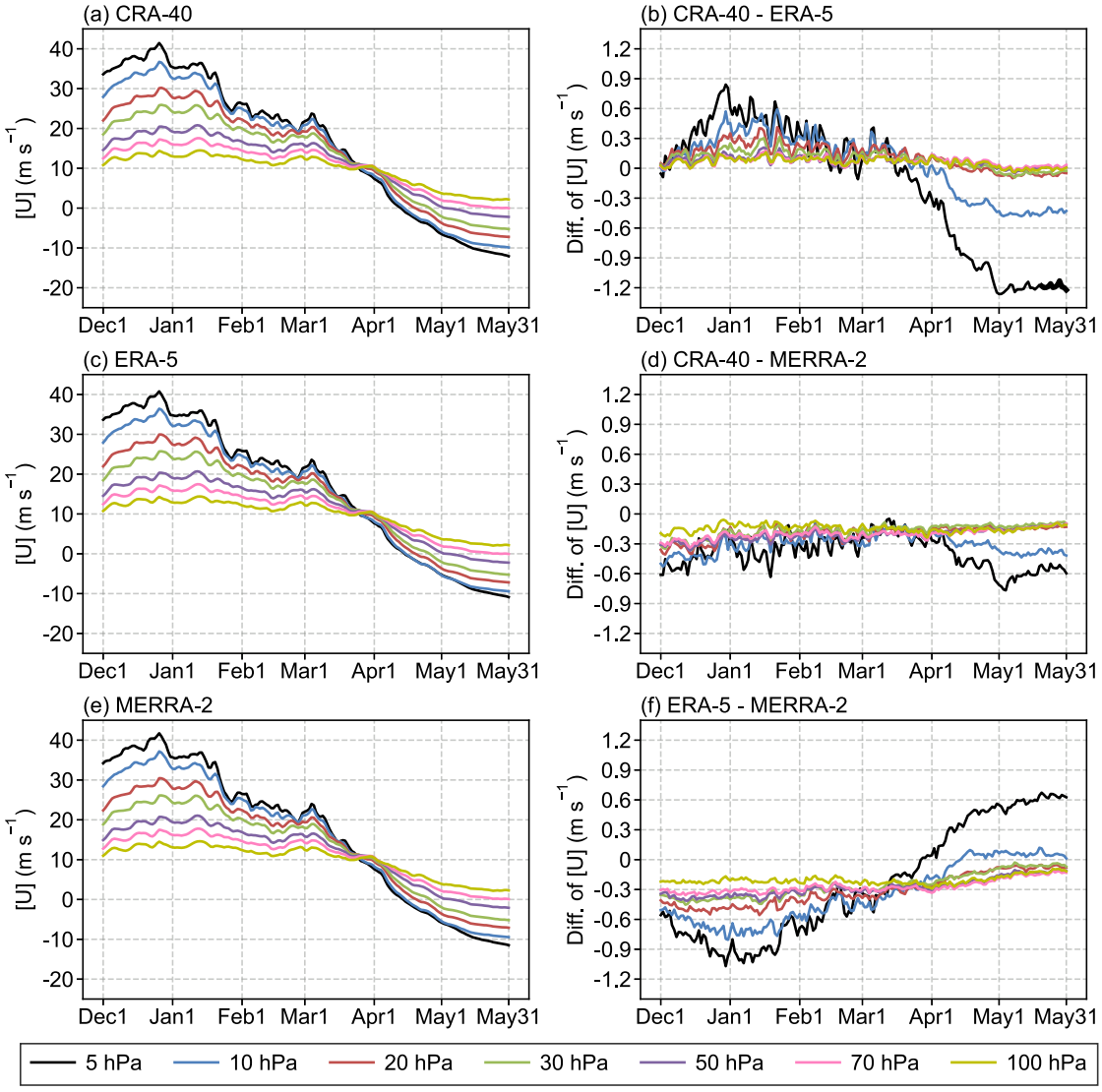

Fig. 3. The daily evolution of the climatological zonal-mean zonal wind in 60°–70°N in (a) CRA-40, (c) ERA-5, and (e) MERRA-2. (b, d, f) As in (a, c, e), but for the difference (d) between CRA-40 and ERA-5, (e) between CRA-40 and MERRA-2, and (f) between ERA-5 and MERRA-2, respectively.

zonal wind in 60°–70°N and temperature over the polar cap (60°–90°N, 0–360°) in the cold season (November–April) from 1981 to 2019 among the three reanalyses. The reanalyses differ from each other regarding the zonal wind in the polar stratosphere before 1999 (Figs. 4a, c, e). The differences between CRA-40 and ERA-5 are smaller in the 1980s than those between CRA-40 and MERRA-2, with an average easterly bias of 1–2 m s^{-1} above 20 hPa in CRA-40 as compared to MERRA-2. In contrast, CRA-40 shares a similar magnitude of zonal wind with MERRA-2 in the 1990s (Fig. 4c). Both CRA-40 and MERRA-2 show a stronger polar night jet than that in ERA-5 with an average westerly bias of 1–2 m s^{-1} at 10 hPa and 5 hPa. However, such differences among the three reanalyses have largely disappeared since 1999, possibly due to the transition from TOVS to ATOVS observations at this time (Long et al., 2017). Corresponding to the differences in the circumpolar zonal wind, cold or warm biases occur frequently in the upper stratosphere in CRA-40 before 1999 as compared to the other two reanalyses. During the period after 1999, the systematic cold biases in the middle and lower stratosphere in CRA-40 have been corrected (Figs. 4b, d); and the main differences between CRA-40 and the other two reanalyses mainly appear at and above 10 hPa with a warm bias of 0.5–1 K at 10 hPa.

3.2.2. *SSW and SFW events*

Large differences among different datasets are often found during the recovery phase after SSWs (Wright and Hindley, 2018). In this section, we examine the onset process of SSWs and SFWs in the Arctic stratosphere. Figure 5 shows the onset dates of SSWs and SFWs at 10 hPa during the period 1981–2019 in the three reanalyses. CRA-40 identifies 22 SSWs with an occurrence frequency of 0.56 events per year (Fig. 5a). ERA-5 and MERRA-2 identify 22 and 21

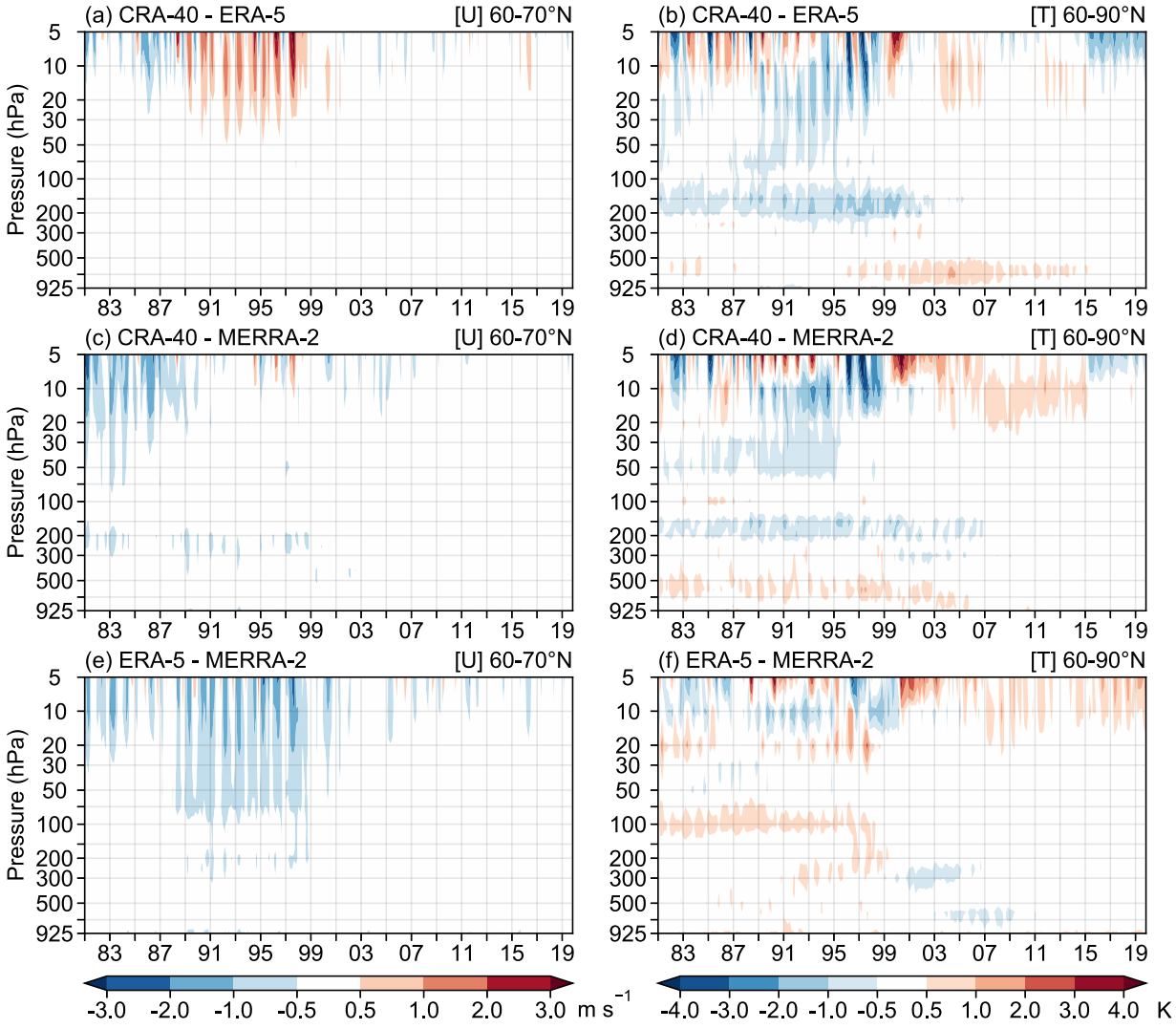

Fig. 4. Monthly difference of (left panels) zonal-mean zonal wind in 60°–70°N and (right panels) temperature over the polar cap (60°–90°N, 0–360°) from November to April, during 1981–2019, (a, b) between CRA-40 and ERA-5, (c, d) between CRA-40 and MERRA-2, and (e, f) between ERA-5 and MERRA-2, respectively.

SSWs following the same method, respectively. Only one SSW event, which occurred in 1981, is not captured by MERRA-2. This is because when the reversal of the zonal wind direction appeared on 4 March 1981 in CRA-40 and ERA-5, a fairly weak westerly wind (~0.2 m s^{-1}) continued to persist on that day in MERRA-2 (figures not shown). If this event is excluded, the SSW onset dates identified by the three reanalyses are quite similar, with 18 events being completely the same, and the other 3 events (SSWs in December 1987, January 2013, and January 2019) featuring a one-day bias. The SFW onset also shows strong agreement among the three reanalyses (Fig. 5b). Specifically, SFWs occur from early March to early May with an average onset date of 14 April in CRA-40, which is one day earlier than those in ERA-5 and MERRA-2. CRA-40 has 29 (32) out 39 years with SFW onset dates identical to ERA-5 (MERRA-2), 9 (6) years with a bias of 1–3 days, and only one year (i.e., 1990) with a bias of up to 5 days. These differences in the SFW onset date mainly appear before 1991. Similar to that of SSWs, the biases of SFW onset date in those specific years are also due to small discrepancies of the circumpolar zonal wind speed around the SFW onset date between CRA-40 and the other two reanalyses. Even in those years, the daily evolution of the 10-hPa circumpolar zonal wind in CRA-40 is highly consistent with that in ERA-5 and MERRA-2 (figures not shown).

Figure 6 shows the height–time evolution of the composite anomalies for the zonal-mean zonal wind in 60°–70°N and temperature averaged over the polar cap from 30 days before to 30 days after the onset date of SSWs in each reanalysis, together with the differences between each pair of reanalyses. CRA-40 can well describe the onset process of SSWs, especially at and below 20 hPa, with the differences from the other two reanalyses mainly located in the stratosphere above 20 hPa, which is consistent with the results in the above sections. Compared to ERA-5, CRA-40 has an easterly

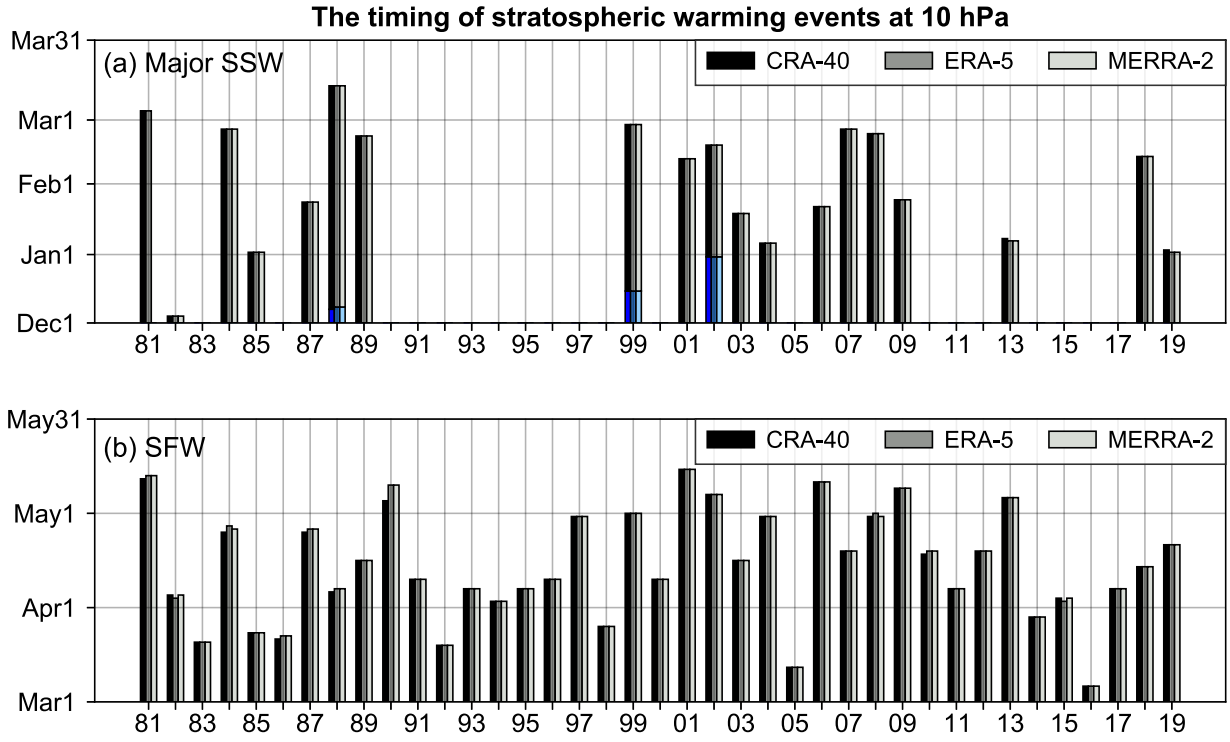

Fig. 5. The 10-hPa onset dates of (a) major SSW and (b) SFW events during 1981–2019 in the three reanalysis datasets. The dark and light blue bars mark the first SSW event in the years in which more than one SSW event occurs in one winter season.

bias of –0.5 to –1.5 m s^{-1} and a warm bias of 0.5 to 0.9 K one month after the occurrence of SSWs (Figs. 6d, j). In contrast, the differences between CRA-40 and MERRA-2 are more scattered (Figs. 6e, k).

Planetary wave activities are crucial for the occurrence of an SSW event (e.g., Polvani and Waugh, 2004; Zhang et al., 2016, 2019; Huang et al., 2017). Figure 7 shows the temporal evolution of the composite vertical component of EP (EP_z) flux of the planetary waves (wavenumbers 1–3) in 55°–75°N in the three reanalyses and their differences. The planetary wave activities in the stratosphere increase drastically from 15 days before the SSW onset and peak 2–3 days before the SSW onset (Figs. 7a–c). There is also a remarkable increase of EP_z flux around 20 days before the SSW onset, which is usually considered as "preconditioning" before a major SSW. Such "preconditioning" weakens the stratospheric polar jet to favor the upward and poleward propagation of planetary waves, creating necessary conditions for the subsequent occurrence of a major SSW (Andrews et al., 1987; Limpasuvan et al., 2004; Manney et al., 2009; Liu et al., 2022). The differences at 20, 30, and 50 hPa are generally consistent in each pair of the reanalyses, indicating a good agreement of CRA-40 with ERA-5 and MERRA-2 in terms of the dynamics during the SSW onset (Figs. 7d–f). However, there are greater differences at 10 hPa. By comparison, the strength of SFW during its onset processes in CRA-40 is much closer to the other two reanalyses (Figs. S3, S4 in the ESM).

The above analyses show that CRA-40 has an excellent performance in characterizing the Arctic stratospheric polar vortex and the polar night jet in winter and spring at and below 10 hPa. Despite the larger differences at 10 hPa between CRA-40 and the other two reanalyses relative to those in the lower layers, CRA-40 is still considered to accurately describe the SSWs and SFWs at this pressure level. In addition, CRA-40 can well characterize the Arctic circulation not only in the stratosphere but also in the troposphere, as shown in Figs. 4 and 6. The Arctic Oscillation (AO), a dominant mode of atmospheric variability over the extratropical Northern Hemisphere (Thompson and Wallace, 1998; Chen et al., 2019; Zheng et al., 2021), has a close relationship with the circulation in the Arctic stratosphere. It is found that CRA-40 can also effectively capture the spatiotemporal features of the AO (figures not shown).

4. The equatorial QBO

4.1. *QBO index*

The above section focuses on the Arctic stratospheric signals in CRA-40. We now turn to the other concern in this study, the equatorial QBO. Figure 8 shows the seasonal and annual mean QBO index in the three reanalyses at different pressure levels for the entire 1981–2019 period. At 5 and 10 hPa, the QBO index in CRA-40 for both annual and seasonal mean shows a westerly bias as compared to ERA-5 (red and black bars in Figs. 8a, b). However, this is not the case for the comparison between CRA-40 and MERRA-2,

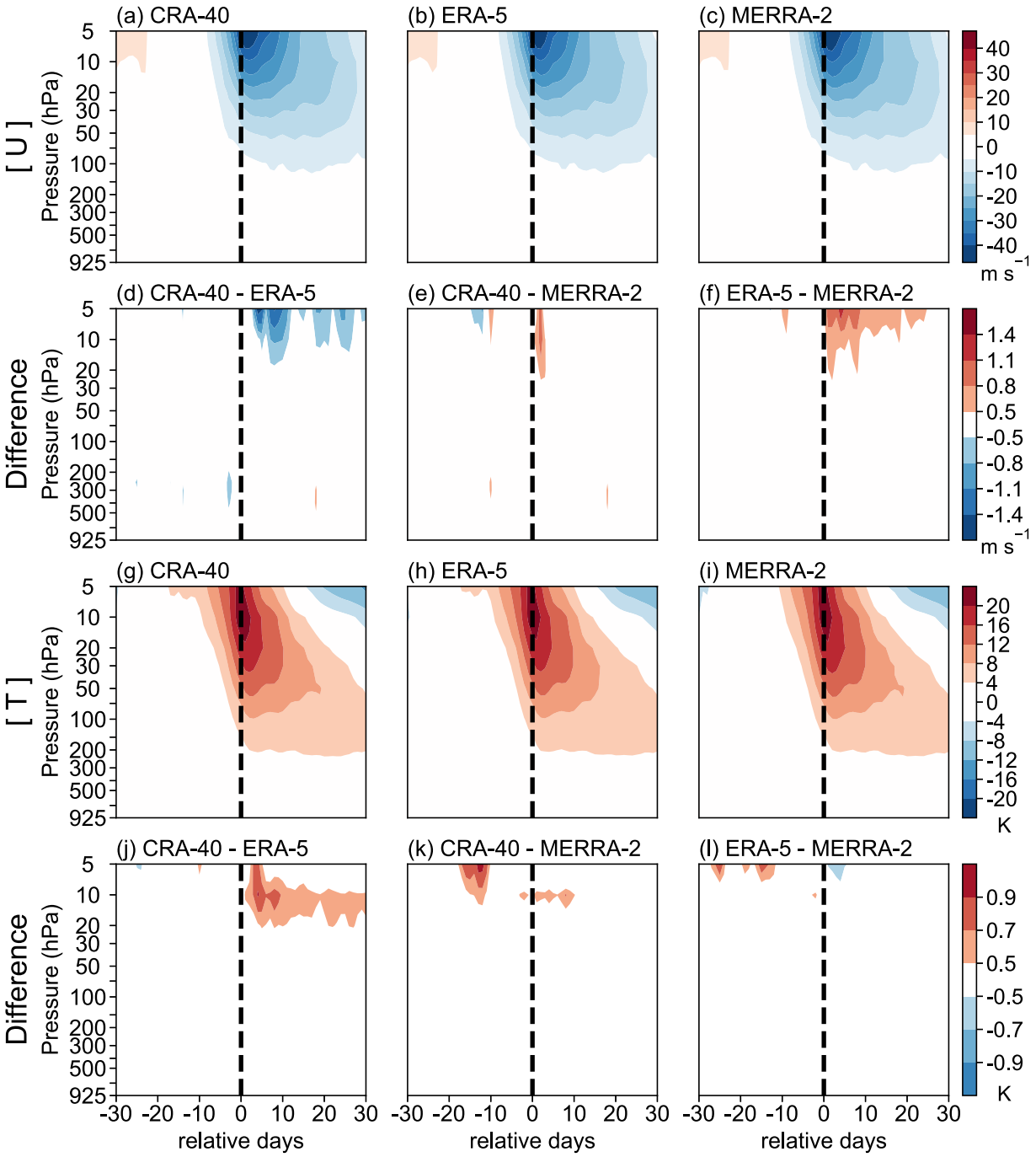

Fig. 6. The height-time evolution of the composite anomalies of (a–c) zonal-mean zonal wind in 60°–70°N from 30 days before to 30 days after the onset date of SSWs in (a) CRA-40, (b) ERA-5, and (c) MERRA-2 and their differences (d) between CRA-40 and ERA-5, (e) between CRA-40 and MERRA-2, and (f) between ERA-5 and MERRA-2, respectively. (g–l) As in (a–f), but for the temperature averaged over the polar cap (60°–90°N, 0°–360°).

which featured westerly biases in winter and spring but easterly biases in summer and autumn (red and gray bars in Figs. 8a, b). Overall, the three reanalyses exhibit substantial disagreement in the QBO index in the upper stratosphere (mainly at 5 hPa). The strength of QBO indices in ERA-5 and MERRA-2 are much closer below 10 hPa (black and gray bars in Figs. 8c–f). However, CRA-40 has clear easterly biases compared with the other two reanalyses at these levels, except for the QBO index in summer and autumn at 50 hPa (Fig. 8e). The maximum easterly bias can reach up to 6.4 m s^{-1} at 30 hPa in summer.

To further compare the QBO index in CRA-40 with ERA-5 and MERRA-2, Fig. 9 shows the monthly QBO index from 1981–2019. The linear trend of the QBO index in CRA-40 is significant at the 99% confidence level at all the selected pressure levels, except at 10 hPa where the signif-

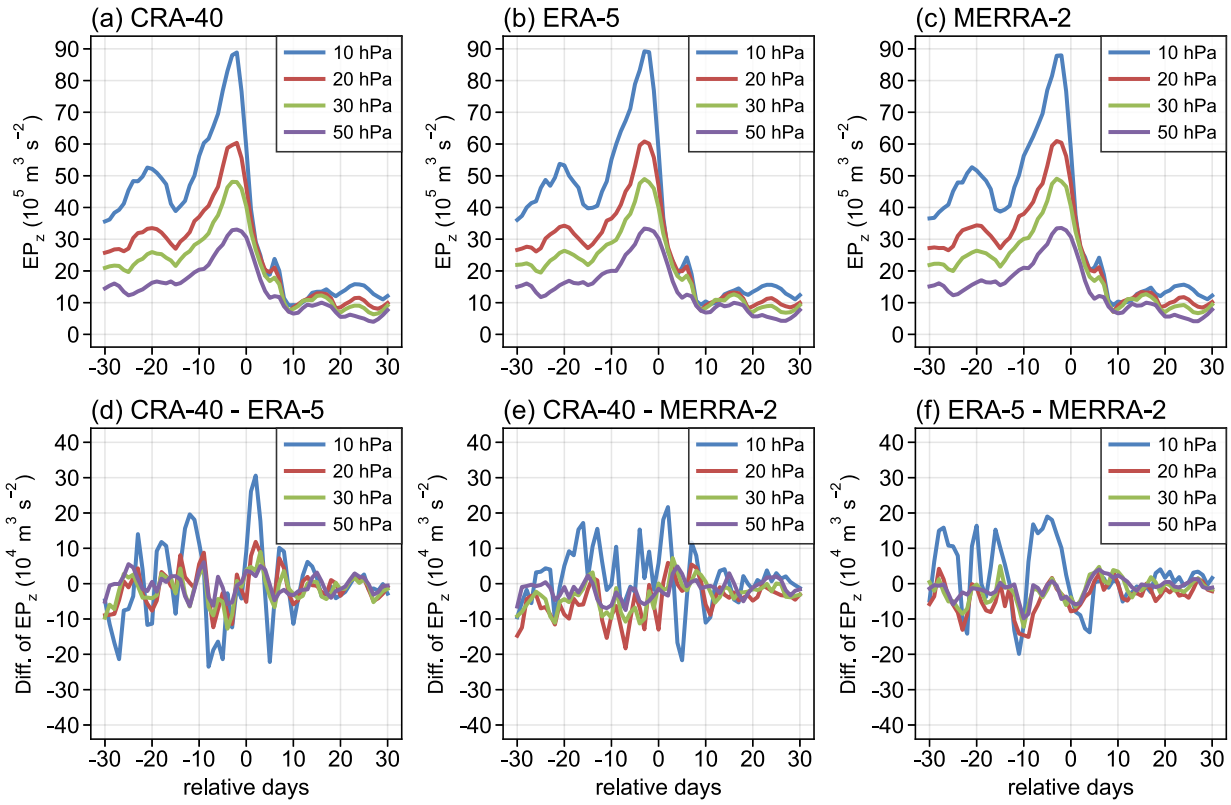

Fig. 7. The temporal evolution of the composite EP_z flux in 55°–75°N relative to the SSW onset in (a) CRA-40, (b) ERA-5, and (c) MERRA-2. (d–f) As in (a–c), but for the difference (d) between CRA-40 and ERA-5, (e) between CRA-40 and MERRA-2, and (f) between ERA-5 and MERRA-2, respectively. The EP_z flux is multiplied by $e^{z/H}$ for clarity. Accordingly, the magnitude of EP_z flux increases with altitude.

icance exceeds the 90% confidence level. However, the QBO index shows a descending trend at 10 and 5 hPa but an increasing trend at other pressure levels, indicating a possible interdecadal change of the QBO in CRA-40. However, ERA-5 shows no significant linear trend except at 20 hPa (Fig. 9h), implying its evident differences from CRA-40. For MERRA-2, the linear trend is seen at 4 out of 6 pressure levels, with a significance exceeding the 90% confidence level.

Considering the significant linear trend in CRA-40, we divide the entire 1981–2019 period into two subperiods, 1981–98 and 1999–2019. The division was chosen because the abrupt change of the monthly QBO index in CRA-40 occurred around 1999 based on the cumulative anomaly method (figures not shown). Meanwhile, the two subperiods correspond well to the TOVS and ATVOS periods in Long et al. (2017), respectively.

Figures 10 and 11 present the difference of the monthly QBO index at different pressure levels in each pair of the three reanalyses during 1981–98 and 1999–2019, respectively. CRA-40 differs significantly from the other two reanalyses during 1981–98 except at 10 hPa when compared to MERRA-2, with an average westerly bias at 5 and 10 hPa and an average easterly bias at other pressure levels (left and middle panels in Fig. 10). In contrast, the differences between ERA-5 and MERRA-2 are insignificant and much smaller, ranging from –16 to 6.3 m s^{-1} below 10 hPa. However, we still see significant differences in the mean QBO index at 5 and 10 hPa (right panels in Fig. 10). During this subperiod, the easterly bias in CRA-40 averaged from 70 to 20 hPa is –5.6 m s^{-1} as compared to ERA-5 and MERRA-2, which is about 65 times that between ERA-5 and MERRA-2.

From 1999–2019, the differences between CRA-40 and the other two reanalyses are substantially reduced from the lower to the upper stratosphere, although they are noticeable at some levels. The easterly bias in CRA-40 averaged from 70 to 20 hPa during this subperiod is approximately 30% that of the former subperiod. However, CRA-40 may have large irregularities at 20 and 30 hPa in 2015 (Figs. 11g, h, j, k). Although ERA-5 has significant easterly biases at 5 and 70 hPa as compared to MERRA-2, they agree more with each other during this subperiod (right panels in Fig. 11).

4.2. *QBO period*

As the QBO is periodic at approximately 28 months (Naujokat, 1986; Baldwin et al., 2001; Richter et al., 2022), we perform a Morlet wavelet analysis to calculate the period of the QBO index in CRA-40. Figure 12 shows the averaged wavelet power spectra of the QBO index during 1981–2019 from 5 to 70 hPa in the three reanalyses. The

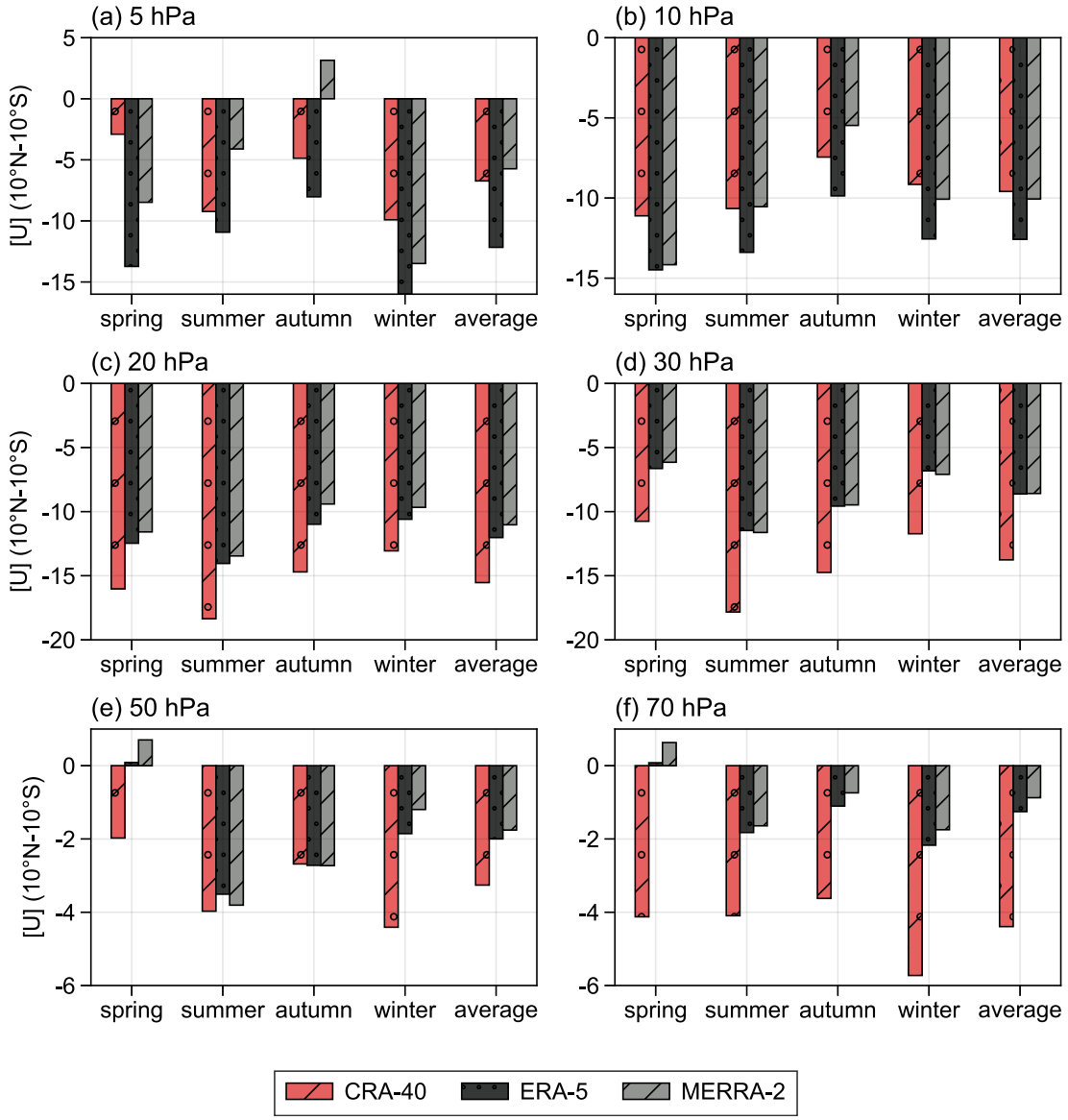

Fig. 8. Seasonal and annual mean QBO index at different pressure levels for the entire 1981–2019 period. Note the smaller increment of the *y*-axis in (e–f).

QBO periods at the selected levels are basically consistent among CRA-40, ERA-5, and MERRA-2, with slight differences that are smaller than 0.4 months. There also exists a noticeable QBO period of ~148 months at 5 hPa in CRA-40 (Fig. 12a). However, the intensity of the wavelet power in CRA-40 is evidently weaker than that in the other two reanalyses from 20 to 70 hPa (Figs. 12g–r). The ratios of the wavelet power intensity between CRA-40 and the other two reanalyses decrease quickly with decreasing height, which amounts to more than 87% at 20 hPa but less than 62% at 70 hPa, highlighting the shortcomings of CRA-40 in characterizing the QBO.

We also examine the interdecadal change of the wavelet power between the subperiod 1981–98 and 1999–2019 (Fig. 13). CRA-40 shows positive biases at 5 hPa (Fig. 13a) and negative biases below 10 hPa (Figs. 13c–f), compared to the other two reanalyses during the first subperiod. However, such biases are largely reduced during the second subperiod except at 30 hPa (Fig. 13d), indicating an improved representation of the QBO in CRA-40 during this subperiod, at least in the lower stratosphere.

4.3. *QBO amplitude*

Figure 14 shows the QBO amplitude during 1981–2019 in the three reanalysis datasets. ERA-5 agrees well with MERRA-2 in terms of QBO amplitude at all the selected levels, especially below 10 hPa where correlation coefficients are higher than 0.8 (gray and black lines in Fig. 14). However, CRA-40 shows considerable disagreement with these two reanalyses at 5 and 10 hPa, with relatively smaller correlation coefficients (Figs. 14a, b). For 20 hPa, although the correlation coefficients between CRA-40 and the other two reanaly-

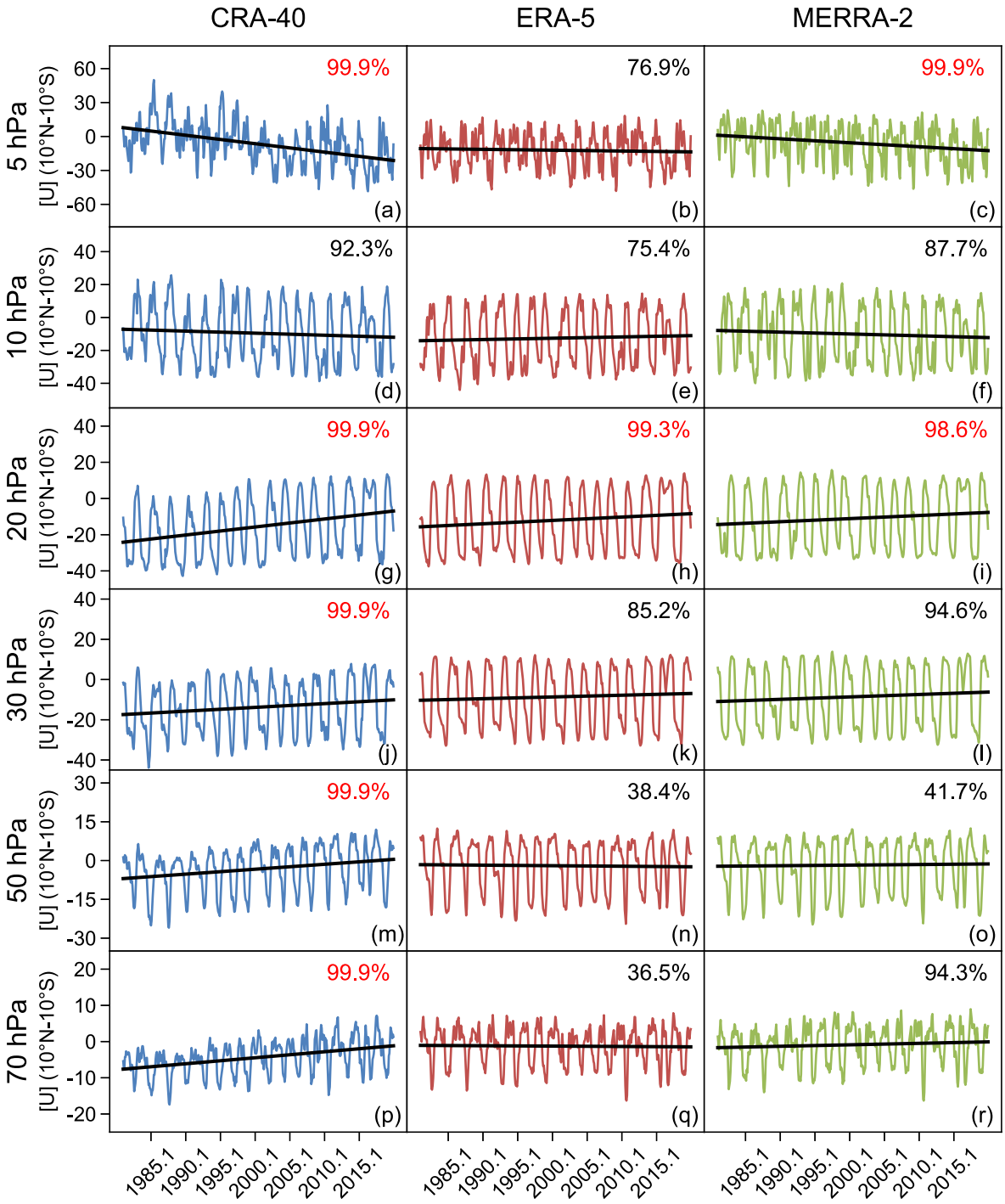

Fig. 9. The monthly QBO index during 1981–2019 at different pressure levels in (left panels) CRA-40, (middle panels) ERA-5, and (right panels) MERRA-2. The black lines represent the linear trends. The percentage in the upper right corner of each panel represents the confidence level of the linear trend, with values higher than 95% marked in red.

ses are still insignificant, the QBO amplitude in CRA-40 agrees well with that in ERA-5 and MERRA-2 since the late 1990s (Fig. 14c); however, it is remarkably weaker than that in ERA-5 and MERRA-2 by about 2.3 m s^{-1} before 1999. At heights below 20 hPa, the QBO amplitude in CRA-40 varies similarly with the other two reanalyses on the interannual time scales (Figs. 14d–f), with the correlation coefficients being more significant than those at 5, 10, and 20 hPa. Nevertheless, the apparently weaker amplitude of QBO is still observed in CRA-40, which is 85.6%, 83.4%, and 82.7% of that in ERA-5 at 30, 50, and 70 hPa, respectively.

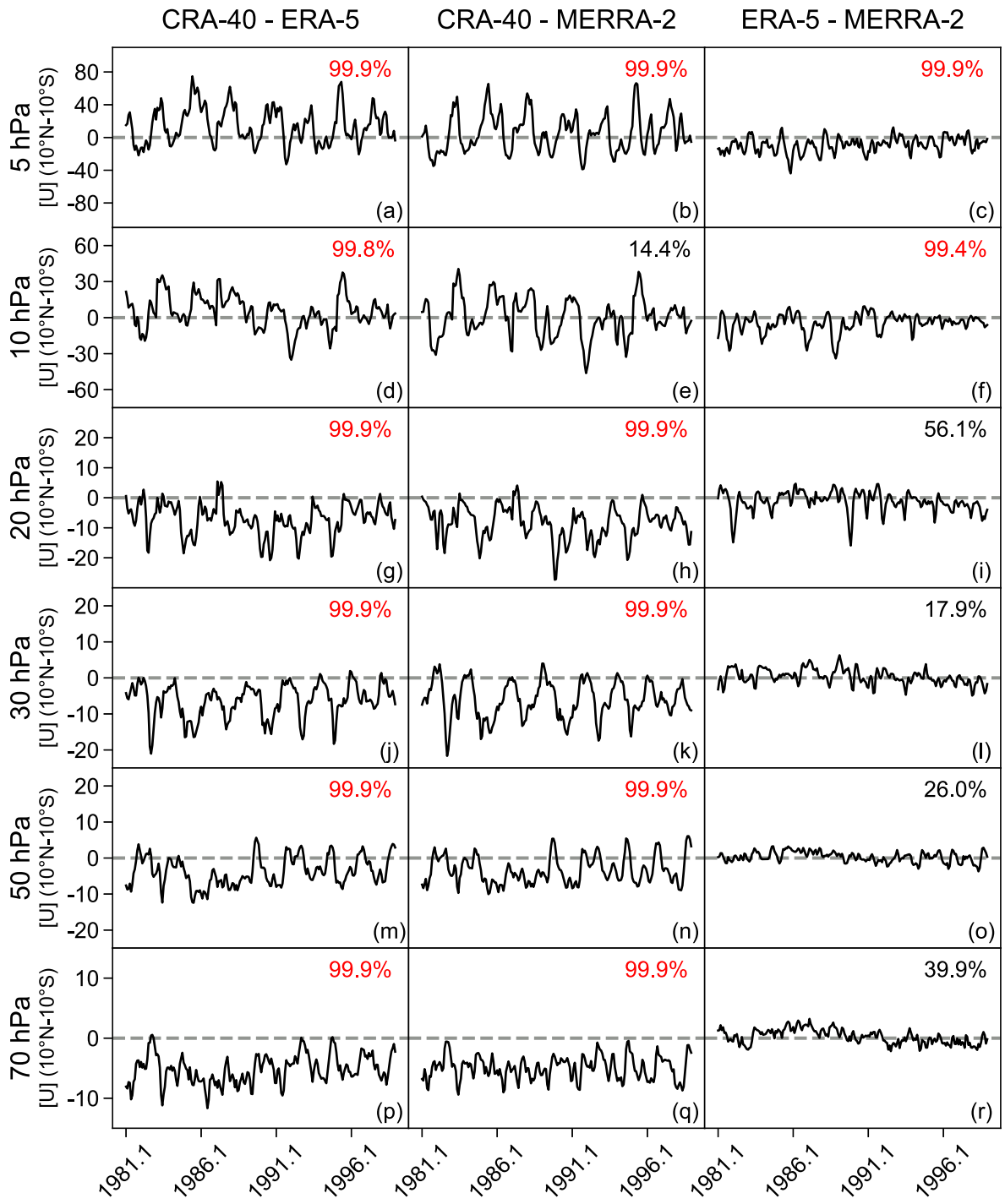

Fig. 10. The difference of the monthly QBO index at different pressure levels during 1981–98: (left panels) between CRA-40 and ERA-5, (middle panels) between CRA-40 and MERRA-2, and (right panels) between ERA-5 and MERRA-2, respectively. The percentage in the upper right corner of each panel represents the confidence level of the difference in the mean QBO index between the two datasets, with values higher than 95% marked in red.

5. Summary and conclusions

This study evaluates the representation of the Arctic stratosphere and the QBO in CRA-40 during 1981–2019 via comparisons with two widely used reanalyses, namely ERA-5 and MERRA-2. The main conclusions are as follows.

CRA-40 can well describe the Arctic stratospheric circulation in winter and spring below 10 hPa. Specifically, CRA-40 has slight differences from ERA-5 and MERRA-2 in terms of the climatological polar-mean temperature (within ±0.5 K) and polar night jet (within ±0.5 m s^{-1}). There are relatively small systematic cold biases in CRA-40 before the

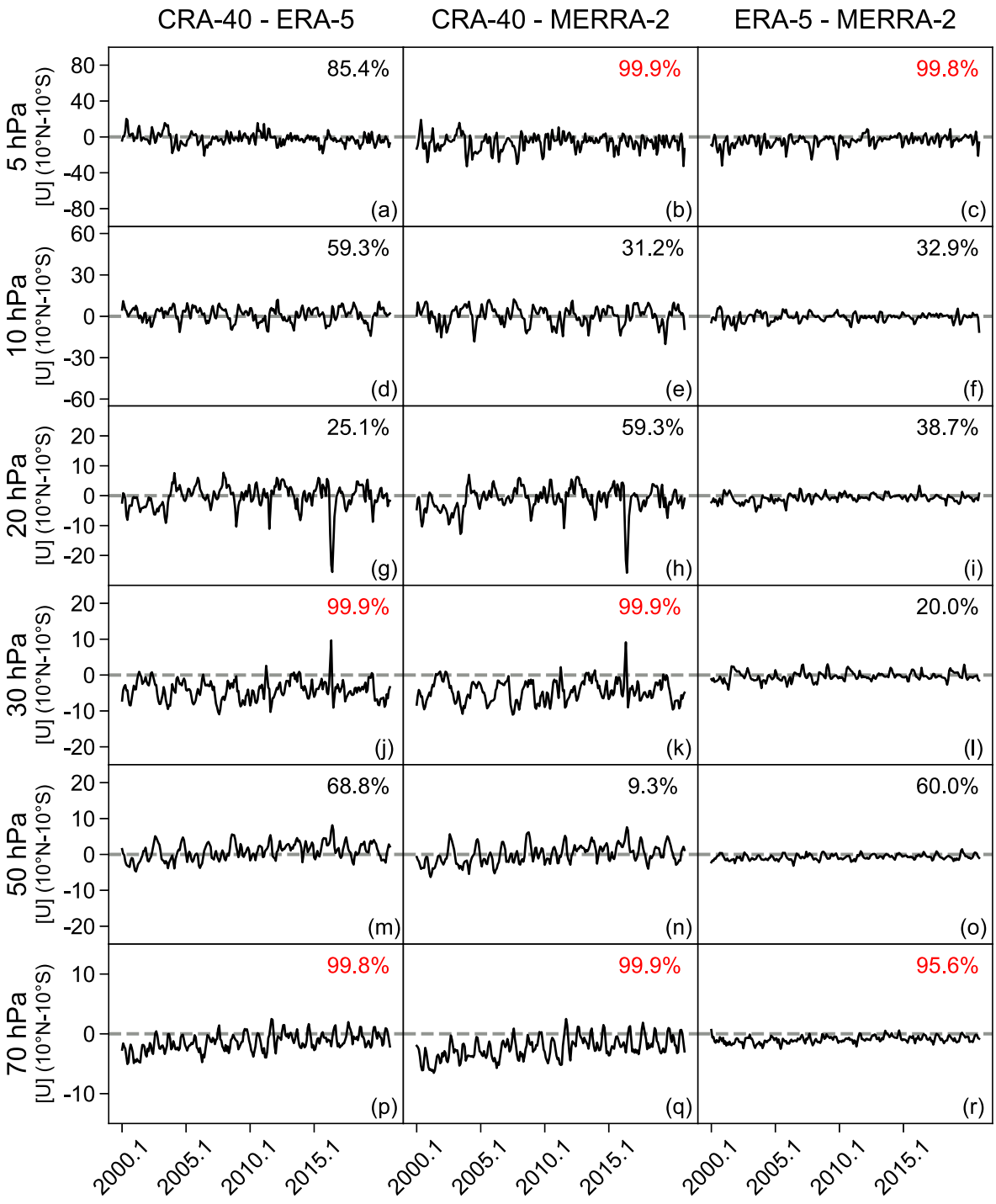

Fig. 11. Same as in Fig. 10, but during 1999–2019.

late 1990s, however, these greatly diminish after 1999 when the ATVOS observations became available. The dynamics and circulation anomalies during the onset process of SSW and SFW events in CRA-40 are also quite close to those in ERA-5 and MERRA-2 with marginal differences.

At 10 hPa, the cold biases of polar temperature in CRA-40 are enlarged during the 1990s, noticeably exceeding –3 K in the late 1990s. After 1999, such biases undergo a sign reversal to warm biases within 0.5–1 K. The SSW onset dates at 10 hPa identified by CRA-40 are relatively identical to ERA-5, with only three SSWs having a one-day bias. Although warmer polar temperature biases appear after the SSW onset and can persist for a month in CRA-40, they range from 0.5 to 0.9 K. The SFW onset date becomes inconsistent among the three reanalyses, but at least 29 out of 39 SFWs share the same onset date. In general, compared to the lower stratospheric levels, the differences at 10 hPa among the three reanalyses increase to a certain extent, but

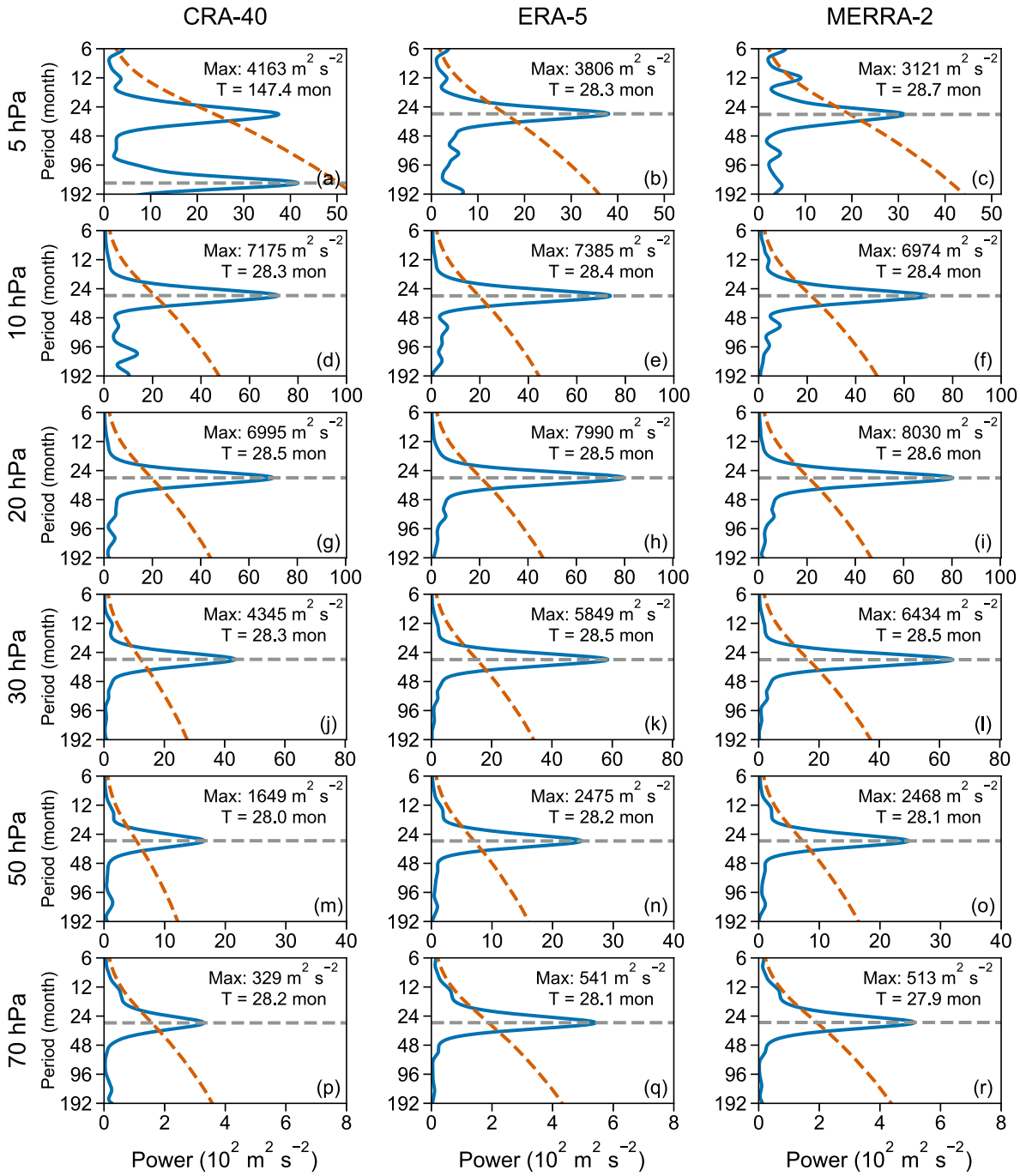

Fig. 12. The averaged wavelet power spectra of the QBO index during 1981–2019 at different pressure levels in (left panels) CRA-40, (middle panels) ERA-5, and (right panels) MERRA-2. The red dashed lines represent the critical value at the 95% confidence level. The values in the upper right corner of each panel give the maximum value of wavelet power spectra and the corresponding QBO period.

within an acceptable range. In contrast, all the reanalyses are highly inconsistent in the upper stratosphere (5 hPa), possibly due to fewer conventional observations available for assimilation.

The differences over the tropics between CRA-40 and the other two reanalyses are much larger than those in the polar region. CRA-40 exhibits pronounced cold and easterly biases below 10 hPa as compared to ERA-5 and MERRA-2. An obvious interdecadal change occurs around 1999 in the QBO of CRA-40, corresponding to the transition from TOVS to ATOVS observations. During 1981–98, CRA-40 performs poorly in characterizing the QBO below 10 hPa relative to the other two reanalyses, shown in terms of larger easterly biases of the QBO index, a weaker amplitude of the QBO, and a weaker wavelet power of the QBO period. However, the performance of CRA-40 is considerably improved

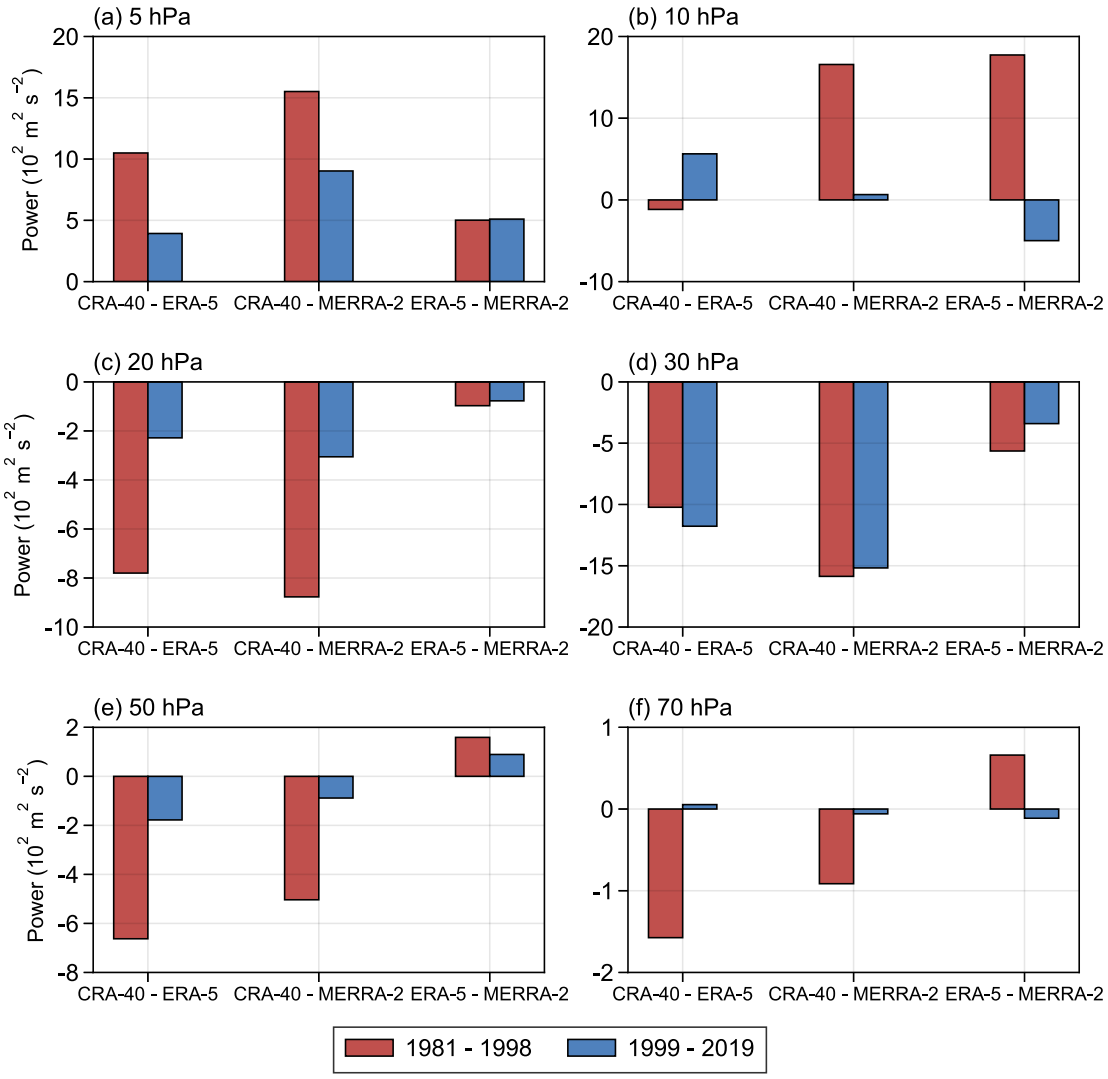

Fig. 13. The difference of the averaged wavelet power spectra of the QBO period between CRA-40 and ERA-5, between CRA-40 and MERRA-2, and between ERA-5 and MERRA-2 at different pressure levels during 1981–98 (red bars) and 1999–2019 (blue bars), respectively.

during 1999–2019. Specifically, the differences in the QBO index, when averaged from 70 to 20 hPa between CRA-40 and the other two reanalyses, have reduced to ~30% of those in the previous subperiod. For the QBO amplitude and the wavelet power of the QBO period, the differences have decreased to ~50% and ~61%, respectively. Nevertheless, compared to the differences between ERA-5 and MERRA-2, the differences between CRA-40 and those two reanalyses are still considerable and cannot be ignored.

The lack of the assimilation of Stratospheric Sounding Unit (SSU) observations may be a reason for the poor representation of QBO in CRA-40 during 1981–98. The radiance channels on SSU are a major source of stratospheric information during the 1980s and 1990s. The SSU instrument forms part of the TOVS suite of instruments and was operational from late-1978 to mid-2006, providing valuable observations of mid-upper stratospheric temperatures in the pre-ATOVS era. MERRA-2 uses version 2.1.3 of the Community Radiative Transfer Model for the assimilation of the satellite radiances including those from SSU (Gelaro et al., 2017). In ERA-5, an improved observation operator has been incorporated for the assimilation of SSU observations (Hersbach et al., 2020). However, the radiance data from SSU is not included in CRA-40, although it will be assimilated into the next generation of CMA's reanalysis data (Liu et al., 2023). Since the early 2000s, more radiance data from AMSU-A that is included in the ATOVS suite of sounding instruments has been assimilated into CRA-40, as well as in MERRA-2 and ERA-5 reanalysis data. This considerably improves the performance of CRA-40 in characterizing the QBO during the period 1999–2019.

Additionally, the tropical stratospheric variability is sensitive to the model top of the atmospheric model used to generate the reanalysis data. Osprey et al. (2013) found an improvement in simulating QBO in high-top (with a model top up to 84 km) configurations of the HadGEM2 model. Rao et al.

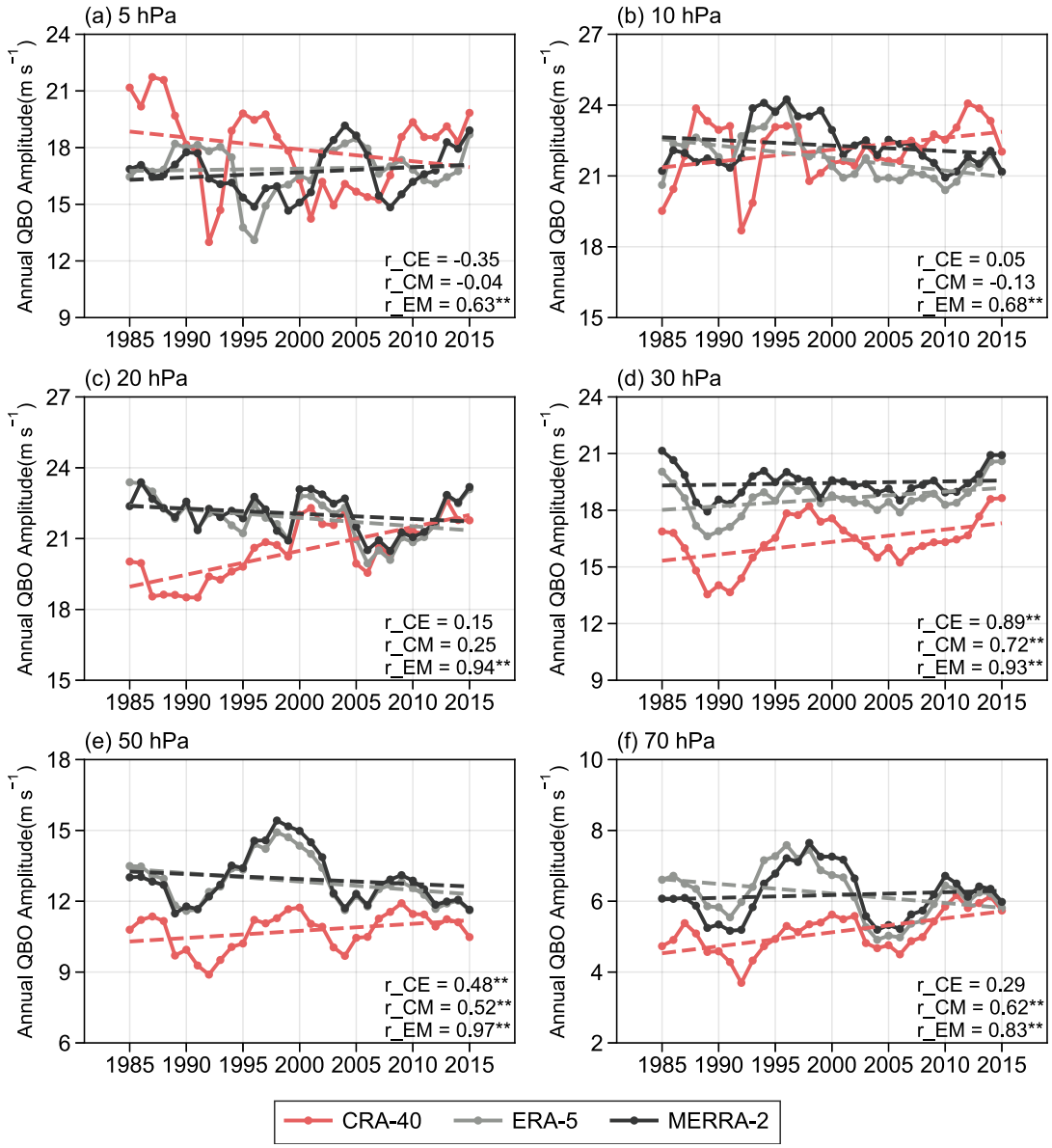

Fig. 14. The QBO amplitude at different pressure levels in the three reanalysis datasets for 1981–2019. The correlation coefficients between CRA-40 and ERA-5 (r_CE), between CRA-40 and MERRA-2 (r_CM), and between ERA-5 and MERRA-2 (r_EM) are given at the lower right corner of each panel. The double asterisks indicate the 95% confidence level for the correlation coefficients. The dashed line represents the linear trend in the corresponding reanalysis.

(2020) also pointed out that most of the CMIP6 models with a QBO are high-top models with a model top at or above the 1-hPa pressure level or higher than ~50 km. Considering that the model tops in both ERA-5 and MERRA-2 reach up to 80 km, the relatively low model top (~55 km) of the atmospheric prediction model used by CRA-40 may also be responsible for its deteriorated representation of QBO.

The findings in this study are consistent with previous studies in that the reanalyses better agree in the polar region than in the tropics and also in the lower stratosphere than in the upper stratosphere (e.g., Long et al., 2017; Wright and Hindley, 2018; Essa et al., 2022). In addition, we only conducted the intercomparison of three reanalyses and did not compare them with observations. Therefore, concluding that one reanalysis is more standardized and reliable than another may be unreasonable. Even the high agreement among the three considered reanalyses cannot imply correctness, as there may be possible similar systematic errors in them. Nevertheless, ERA-5 and MERRA-2 can better characterize the circulation in the lower and middle stratosphere, as reported previously (e.g., Coy et al., 2016; Kawatani et al., 2016; Pahlavan et al., 2021; Essa et al., 2022). Given this, the comparisons of CRA-40 with these two reanalyses in this study are reliable to a large degree; that is, while CRA-40 can well characterize the winter and spring circulation in the lower and middle Arctic stratosphere, it cannot

yet describe the equatorial QBO well. Thus, improving the representation of equatorial winds by assimilating more satellite radiance data, for example, those from SSU in the 1980s and 1990s, is one of the essential tasks for the next generation of CMA's reanalysis data.

Data availability CRA-40 data were downloaded from the web site http://data.cma.cn/data/cdcdetail/dataCode/NAFP_CRA40_FTM_DAY.html. ERA-5 data were downloaded from the web site https://www.ecmwf.int/en/forecasts/datasets/reanalysis-datasets/era5. MERRA-2 data were downloaded from https://disc.gsfc.nasa.gov/datasets?project=MERRA-2.

Acknowledgments We thank the two anonymous reviewers and the editors for their assistance in evaluating this paper. This work was supported by the National Natural Science Foundation of China (Grant Nos. 41975048, 42030605, and 42175069), the Natural Science Foundation of Jiangsu Province (Grant No. BK20191404). We thank Mr. Xiang GAO for processing parts of the reanalyses data.

Electronic supplementary material: Supplementary material is available in the online version of this article at https://doi.org/10.1007/s00376-023-3127-1.

Appendix: Major Abbreviations

3D-Var three-dimensional variational (**4D-Var** for four-dimensional variational)
AMSU-A Advanced Microwave Sounding Unit-A
ATOVS Advanced TIROS Operational Vertical Sounder
CMA China Meteorological Administration
CMIP6 Coupled Model Intercomparison Project phase 6
DOE Department of Energy
ECMWF European Centre for Medium-Range Weather Forecasts
ERA-40 ECMWF 40-year reanalysis
ERA-5 ECMWF Reanalysis version 5
GMAO Global Modeling and Assimilation Office of NASA
GOES Geostationary Operational Environmental Satellite
HadGEM2 Hadley Centre Global Environmental Model version 2
JRA-55 Japanese 55-year reanalysis
MERRA-2 Modern Era Retrospective-Analysis for Research version 2
NASA National Aeronautics and Space Administration
NCAR National Center for Atmospheric Research
NCEP National Centers for Environmental Prediction
NCEP-1 NCEP-NCAR Reanalysis 1
NCEP-2 NCEP-DOE Reanalysis 2
NMIC National Meteorological Information Center of the CMA
QBO quasi-biennial oscillation
SFW stratospheric final warming
SPARC Stratosphere–troposphere Processes And their Role in Climate
SSU Stratospheric Sounding Unit
SSW stratospheric sudden warming
TIROS Television Infrared Observation Satellite
TOVS TIROS Operational Vertical Sounder

REFERENCES

Andrews, D. G., J. R. Holton, and C. B. Leovy, 1987: *Middle Atmosphere Dynamics*. Academic Press, 489 pp.

Angell, J. K., and J. Korshover, 1964: Quasi-biennial variations in temperature, total ozone, and tropopause height. *J. Atmos. Sci.*, **21**, 479–492, https://doi.org/10.1175/1520-0469(1964)021<0479:QBVITT>2.0.CO;2.

Ayarzagüena, B., and E. Serrano, 2009: Monthly characterization of the tropospheric circulation over the Euro-Atlantic area in relation with the timing of stratospheric final warmings. *J. Climate*, **22**, 6313–6324, https://doi.org/10.1175/2009JCLI2913.1.

Baldwin, M. P., and T. J. Dunkerton, 2001: Stratospheric harbingers of anomalous weather regimes. *Science*, **294**, 581–584, https://doi.org/10.1126/science.1063315.

Baldwin, M. P., and Coauthors, 2001: The quasi-biennial oscillation. *Rev. Geophys.*, **39**, 179–229, https://doi.org/10.1029/1999RG000073.

Baldwin, M. P., D. B. Stephenson, D. W. J. Thompson, T. J. Dunkerton, A. J. Charlton, and A. O'Neill, 2003: Stratospheric memory and skill of extended-range weather forecasts. *Science*, **301**, 636–640, https://doi.org/10.1126/science.1087143.

Baldwin, M. P., and Coauthors, 2021: Sudden stratospheric warmings. *Rev. Geophys.*, **59**, e2020RG000708, https://doi.org/10.1029/2020RG000708.

Black, R. X., and B. A. McDaniel, 2007a: Interannual variability in the Southern Hemisphere circulation organized by stratospheric final warming events. *J. Atmos. Sci.*, **64**, 2968–2974, https://doi.org/10.1175/JAS3979.1.

Black, R. X., and B. A. McDaniel, 2007b: The dynamics of Northern Hemisphere stratospheric final warming events. *J. Atmos. Sci.*, **64**, 2932–2946, https://doi.org/10.1175/JAS3981.1.

Black, R. X., B. A. McDaniel, and W. A. Robinson, 2006: Stratosphere-troposphere coupling during spring onset. *J. Climate*, **19**, 4891–4901, https://doi.org/10.1175/jcli3907.1.

Cai, Q. Y., W. Chen, S. F. Chen, T. J. Ma, and C. I. Garfinkel, 2022: Influence of the Quasi-Biennial Oscillation on the spatial structure of the wintertime Arctic Oscillation. *J. Geophys. Res.*, **127**, e2021JD035564, https://doi.org/10.1029/2021JD035564.

Charlton, A. J., and L. M. Polvani, 2007: A new look at stratospheric sudden warmings. Part I: Climatology and modeling benchmarks. *J. Climate*, **20**, 449–469, https://doi.org/10.1175/jcli3996.1.

Chen, S. F., R. G. Wu, W. Chen, and L. Y. Song, 2019: Performance of the CMIP5 models in simulating the Arctic Oscillation during boreal spring. *Climate Dyn.*, **53**, 2083–2101, https://doi.org/10.1007/s00382-019-04792-3.

Coy, L., K. Wargan, A. M. Molod, W. R. McCarty, and S. Pawson, 2016: Structure and dynamics of the Quasi-Biennial Oscillation in MERRA-2. *J. Climate*, **29**, 5339–5354, https://

doi.org/10.1175/JCLI-D-15-0809.1.

Dunkerton, T. J., 1997: The role of gravity waves in the quasi-biennial oscillation. *J. Geophys. Res.*, **102**, 26 053–26 076, https://doi.org/10.1029/96JD02999.

Ebdon, R. A., 1960: Notes on the wind flow at 50 mb in tropical and sub-tropical regions in January 1957 and January 1958. *Quart. J. Roy. Meteor. Soc.*, **86**, 540–542, https://doi.org/10.1002/qj.49708637011.

Ebdon, R. A., and R. G. Veryard, 1961: Fluctuations in equatorial stratospheric winds. *Nature*, **189**, 791–793, https://doi.org/10.1038/189791a0.

Essa, Y. H., C. Cagnazzo, F. Madonna, P. Cristofanelli, C. X. Yang, F. Serva, L. Caporaso, and R. Santoleri, 2022: Intercomparison of atmospheric upper-air temperature from recent global reanalysis datasets. *Frontiers in Earth Science*, **10**, 935139, https://doi.org/10.3389/feart.2022.935139.

Fujiwara, M., and Coauthors, 2017: Introduction to the SPARC Reanalysis Intercomparison Project (S-RIP) and overview of the reanalysis systems. *Atmospheric Chemistry and Physics*, **17**, 1417–1452, https://doi.org/10.5194/acp-17-1417-2017.

Gelaro, R., and Coauthors, 2017: The modern-era retrospective analysis for research and applications, version 2 (MERRA-2). *J. Climate*, **30**, 5419–5454, https://doi.org/10.1175/jcli-d-16-0758.1.

Giorgetta, M. A., E. Manzini, and E. Roeckner, 2002: Forcing of the quasi-biennial oscillation from a broad spectrum of atmospheric waves. *Geophys. Res. Lett.*, **29**, 1245, https://doi.org/10.1029/2002GL014756.

Gray, L. J., J. A. Anstey, Y. Kawatani, H. Lu, S. Osprey, and V. Schenzinger, 2018: Surface impacts of the Quasi Biennial Oscillation. *Atmospheric Chemistry and Physics*, **18**, 8227–8247, https://doi.org/10.5194/acp-18-8227-2018.

Hall, R. J., D. M. Mitchell, W. J. M. Seviour, and C. J. Wright, 2022: How well are sudden stratospheric warming surface impacts captured in CMIP6 climate models. *J. Geophys. Res.*, **127**, e2021JD035725, https://doi.org/10.1029/2021JD035725.

Hersbach, H., and Coauthors, 2020: The ERA5 global reanalysis. *Quart. J. Roy. Meteor. Soc.*, **146**, 1999–2049, https://doi.org/10.1002/qj.3803.

Holton, J. R., and R. S. Lindzen, 1972: An updated theory for the quasi-biennial cycle of the tropical stratosphere. *J. Atmos. Sci.*, **29**, 1076–1080, https://doi.org/10.1175/1520-0469(1972)029<1076:AUTFTQ>2.0.CO;2.

Hu, J. G., and R. C. Ren, 2018: Stratospheric control of the Indian Summer Monsoon onset. *Dyn. Atmos. Oceans*, **83**, 135–147, https://doi.org/10.1016/j.dynatmoce.2018.07.004.

Hu, J. G., R. C. Ren, and H. M. Xu, 2014: Occurrence of winter stratospheric sudden warming events and the seasonal timing of spring stratospheric final warming. *J. Atmos. Sci.*, **71**, 2319–2334, https://doi.org/10.1175/JAS-D-13-0349.1.

Hu, J. G., T. M. Li, and H. M. Xu, 2018: Relationship between the North Pacific Gyre Oscillation and the onset of stratospheric final warming in the northern Hemisphere. *Climate Dyn.*, **51**, 3061–3075, https://doi.org/10.1007/s00382-017-4065-3.

Huang, J. L., W. S. Tian, J. K. Zhang, Q. Huang, H. Y. Tian, and J. L. Luo, 2017: The connection between extreme stratospheric polar vortex events and tropospheric blockings. *Quart. J. Roy. Meteor. Soc.*, **143**, 1148–1164, https://doi.org/10.1002/qj.3001.

Huangfu, J. L., Y. L. Tang, L. Wang, W. Chen, R. H. Huang, and T. J. Ma, 2022: Joint influence of the quasi-biennial oscillation and Indian Ocean basin mode on tropical cyclone occurrence frequency over the western North Pacific. *Climate Dyn.*, **59**, 3439–3449, https://doi.org/10.1007/s00382-022-06276-3.

Kawatani, Y., and K. Hamilton, 2013: Weakened stratospheric quasibiennial oscillation driven by increased tropical mean upwelling. *Nature*, **497**, 478–481, https://doi.org/10.1038/nature12140.

Kawatani, Y., K. Hamilton, K. Miyazaki, M. Fujiwara, and J. A. Anstey, 2016: Representation of the tropical stratospheric zonal wind in global atmospheric reanalyses. *Atmospheric Chemistry and Physics*, **16**, 6681–6699, https://doi.org/10.5194/acp-16-6681-2016.

Li, L., C. Y. Li, J. Pan, and Y. K. Tan, 2012: On the differences and climate impacts of early and late stratospheric polar vortex breakup. *Adv. Atmos. Sci.*, **29**, 1119–1128, https://doi.org/10.1007/s00376-012-1012-4.

Liang, X., L. P. Jiang, Y. Pan, C. X. Shi, Z. Q. Liu, and Z. J. Zhou, 2020: A 10-Yr global land surface reanalysis interim dataset (CRA-Interim/Land): Implementation and preliminary evaluation. *Journal of Meteorological Research*, **34**, 101–116, https://doi.org/10.1007/s13351-020-9083-0.

Limpasuvan, V., D. W. J. Thompson, and D. L. Hartmann, 2004: The life cycle of the Northern Hemisphere sudden stratospheric warmings. *J. Climate*, **17**, 2584–2596, https://doi.org/10.1175/1520-0442(2004)017<2584:TLCOTN>2.0.CO;2.

Lindzen, R. S., and J. R. Holton, 1968: A theory of the Quasi-Biennial Oscillation. *J. Atmos. Sci.*, **25**, 1095–1107, https://doi.org/10.1175/1520-0469(1968)025<1095:ATOTQB>2.0.CO;2.

Liu, G. Y., T. Hirooka, N. Eguchi, and K. Krüger, 2022: Dynamical evolution of a minor sudden stratospheric warming in the Southern Hemisphere in 2019. *Atmospheric Chemistry and Physics*, **22**, 3493–3505, https://doi.org/10.5194/acp-22-3493-2022.

Liu, Z. Q., and Coauthors, 2017: CMA global reanalysis (CRA-40): Status and plans. *Proc. 5th Int. Conf. on Reanalysis*, Rome, Italy, National Meteorological Information Center, 1–16.

Liu, Z. Q., and Coauthors, 2023: CRA-40/Atmosphere–the first-generation Chinese atmospheric reanalysis (1979–2018): System description and performance evaluation. *Journal of Meteorological Research*, **37**, 1–19, https://doi.org/10.1007/s13351-023-2086-x.

Long, C. S., M. Fujiwara, S. Davis, D. M. Mitchell, and C. J. Wright, 2017: Climatology and interannual variability of dynamic variables in multiple reanalyses evaluated by the SPARC Reanalysis Intercomparison Project (S-RIP). *Atmospheric Chemistry and Physics*, **17**, 14 593–14 629, https://doi.org/10.5194/acp-17-14593-2017.

Manney, G. L., and Coauthors, 2005a: Diagnostic comparison of meteorological analyses during the 2002 Antarctic winter. *Mon. Wea. Rev.*, **133**, 1261–1278, https://doi.org/10.1175/MWR2926.1.

Manney, G. L., K. Krüger, J. L. Sabutis, S. A. Sena, and S. Pawson, 2005b: The remarkable 2003-2004 winter and other recent warm winters in the Arctic stratosphere since the late 1990s. *J. Geophys. Res.*, **110**, D04107, https://doi.org/10.1029/2004jd005367.

Manney, G. L., and Coauthors, 2009: Aura Microwave Limb Sounder observations of dynamics and transport during the

record-breaking 2009 Arctic stratospheric major warming. *Geophys. Res. Lett.*, **36**, L12815, https://doi.org/10.1029/2009GL038586.

Martineau, P., and S. W. Son, 2010: Quality of reanalysis data during stratospheric vortex weakening and intensification events. *Geophys. Res. Lett.*, **37**, L22801, https://doi.org/10.1029/2010GL045237.

Matsuno, T., 1971: A dynamical model of the stratospheric sudden warming. *J. Atmos. Sci.*, **28**, 1479–1494, https://doi.org/10.1175/1520-0469(1971)028<1479:ADMOTS>2.0.CO;2.

McDaniel, B. A., and R. X. Black, 2005: Intraseasonal dynamical evolution of the Northern annular mode. *J. Climate*, **18**, 3820–3839, https://doi.org/10.1175/JCLI3467.1.

McInturff R. M., 1978: Stratospheric warmings: Synoptic, dynamic and general-circulation aspects. NASA Reference Publication 1017, 174 pp.

Naujokat, B., 1986: An update of the observed Quasi-Biennial Oscillation of the stratospheric winds over the tropics. *J. Atmos. Sci.*, **43**, 1873–1877, https://doi.org/10.1175/1520-0469(1986)043<1873:Auotoq>2.0.Co;2.

Osprey, S. M., L. J. Gray, S. C. Hardiman, N. Butchart, and T. J. Hinton, 2013: Stratospheric variability in twentieth-century CMIP5 simulations of the Met Office climate model: HIGH top versus low Top. *J. Climate*, **26**, 1595–1606, https://doi.org/10.1175/JCLI-D-12-00147.1.

Pahlavan, H. A., Q. Fu, J. M. Wallace, and G. N. Kiladis, 2021: Revisiting the Quasi-Biennial Oscillation as seen in ERA5. Part I: Description and momentum budget. *J. Atmos. Sci.*, **78**, 673–691, https://doi.org/10.1175/JAS-D-20-0248.1.

Pawson, S., and M. Fiorino, 1998: A comparison of reanalyses in the tropical stratosphere. Part 1: Thermal structure and the annual cycle. *Climate Dyn.*, **14**, 631–644, https://doi.org/10.1007/s003820050246.

Pawson, S., and M. Fiorino, 1999: A comparison of reanalyses in the tropical stratosphere. Part 3: Inclusion of the pre-satellite data era. *Climate Dyn.*, **15**, 241–250, https://doi.org/10.1007/s003820050279.

Polvani, L. M., and D. W. Waugh, 2004: Upward wave activity flux as a precursor to extreme stratospheric events and subsequent anomalous surface weather regimes. *J. Climate*, **17**, 3548–3554, https://doi.org/10.1175/1520-0442(2004)017<3548:UWAFAA>2.0.CO;2.

Randel, W., and Coauthors, 2004: The SPARC intercomparison of middle-atmosphere climatologies. *J. Climate*, **17**, 986–1003, https://doi.org/10.1175/1520-0442(2004)017<0986:TSIOMC>2.0.CO;2.

Rao, J., C. I. Garfinkel, and I. P. White, 2020: How does the Quasi-Biennial Oscillation affect the boreal winter tropospheric circulation in CMIP5/6 models. *J. Climate*, **33**, 8975–8996, https://doi.org/10.1175/JCLI-D-20-0024.1.

Rao, J., and C. I. Garfinkel, 2021: Projected changes of stratospheric final warmings in the Northern and Southern Hemispheres by CMIP5/6 models. *Climate Dyn.*, **56**, 3353–3371, https://doi.org/10.1007/s00382-021-05647-6.

Rao, J., C. I. Garfinkel, and I. P. White, 2021: Development of the extratropical response to the stratospheric Quasi-Biennial Oscillation. *J. Climate*, **34**, 7239–7255, https://doi.org/10.1175/JCLI-D-20-0960.1.

Reed, R. J., 1964: A tentative model of the 26-month oscillation in tropical latitudes. *Quart. J. Roy. Meteor. Soc.*, **90**, 441–466, https://doi.org/10.1002/qj.49709038607.

Reed, R. J., W. J. Campbell, L. A. Rasmussen, and D. G. Rogers, 1961: Evidence of a downward-propagating, annual wind reversal in the equatorial stratosphere. *J. Geophys. Res.*, **66**, 813–818, https://doi.org/10.1029/JZ066i003p00813.

Ren, R. C., and J. G. Hu, 2014: An emerging precursor signal in the stratosphere in recent decades for the Indian summer monsoon onset. *Geophys. Res. Lett.*, **41**, 7391–7396, https://doi.org/10.1002/2014gl061633.

Richter, J. H., and Coauthors, 2022: Response of the Quasi-Biennial Oscillation to a warming climate in global climate models. *Quart. J. Roy. Meteor. Soc.*, **148**, 1490–1518, https://doi.org/10.1002/qj.3749.

Shen, C., J. L. Zha, J. Wu, D. M. Zhao, C. Azorin-Molina, W. X. Fan, and Y. Yu, 2022: Does CRA-40 outperform other reanalysis products in evaluating near-surface wind speed changes over China. *Atmospheric Research*, **266**, 105948, https://doi.org/10.1016/j.atmosres.2021.105948.

Simmons, A. J., P. Poli, D. P. Dee, P. Berrisford, H. Hersbach, S. Kobayashi, and C. Peubey, 2014: Estimating low-frequency variability and trends in atmospheric temperature using ERA-Interim. *Quart. J. Roy. Meteor. Soc.*, **140**, 329–353, https://doi.org/10.1002/qj.2317.

Thompson, D. W. J., and J. M. Wallace, 1998: The Arctic oscillation signature in the wintertime geopotential height and temperature fields. *Geophys. Res. Lett.*, **25**, 1297–1300, https://doi.org/10.1029/98GL00950.

Wang, L., L. Wang, W. Chen, and J. L. Huangfu, 2021: Modulation of winter precipitation associated with tropical cyclone of the western North Pacific by the stratospheric Quasi-Biennial oscillation. *Environmental Research Letters*, **16**, 054004, https://doi.org/10.1088/1748-9326/abf3dd.

Waugh, D. W., and P.-P. Rong, 2002: Interannual variability in the decay of lower stratospheric Arctic vortices. *J. Meteor. Soc. Japan*, **80**, 997–1012, https://doi.org/10.2151/jmsj.80.997.

Waugh, D. W., W. J. Randel, S. Pawson, P. A. Newman, and E. R. Nash, 1999: Persistence of the lower stratospheric polar vortices. *J. Geophys. Res.*, **104**, 27 191–27 201, https://doi.org/10.1029/1999JD900795.

Wei, K., W. Chen, and R. H. Huang, 2007: Dynamical diagnosis of the breakup of the stratospheric polar vortex in the Northern Hemisphere. *Science in China Series D: Earth Sciences*, **50**, 1369–1379, https://doi.org/10.1007/s11430-007-0100-2.

Wright, C. J., and N. P. Hindley, 2018: How well do stratospheric reanalyses reproduce high-resolution satellite temperature measurements? *Atmospheric Chemistry and Physics*, **18**, 13 703–13 731, https://doi.org/10.5194/acp-18-13703-2018.

Xie, F., and Coauthors, 2018: Effect of the Indo-Pacific warm pool on lower-stratospheric water vapor and comparison with the effect of ENSO. *J. Climate*, **31**, 929–943, https://doi.org/10.1175/jcli-d-17-0575.1.

Xie, F., J. K. Zhang, X. T. Li, J. Li, T. Wang, and M. Xu, 2020: Independent and joint influences of eastern Pacific El Niño-southern oscillation and quasi-biennial oscillation on Northern Hemispheric stratospheric ozone. *International Journal of Climatology*, **40**, 5289–5307, https://doi.org/10.1002/joc.6519.

Yang, J. X., M. T. Huang, and P. M. Zhai, 2021: Performance of the CRA-40/Land, CMFD, and ERA-Interim datasets in reflecting changes in surface air temperature over the Tibetan Plateau. *Journal of Meteorological Research*, **35**, 663–672, https://doi.org/10.1007/s13351-021-0196-x.

Zhang, J. K., W. S. Tian, M. P. Chipperfield, F. Xie, and J. L. Huang, 2016: Persistent shift of the Arctic polar vortex

towards the Eurasian continent in recent decades. *Nature Climate Change*, **6**, 1094–1099, https://doi.org/10.1038/nclimate3136.

Zhang, J. K., F. Xie, Z. C. Ma, C. Y. Zhang, M. Xu, T. Wang, and R. H. Zhang, 2019: Seasonal evolution of the Quasi-biennial Oscillation impact on the Northern Hemisphere polar vortex in winter. *J. Geophys. Res.*, **124**, 12 568–12 586, https://doi.org/10.1029/2019JD030966.

Zhang, R. H., W. S. Tian, and T. Wang, 2020: Role of the quasi-biennial oscillation in the downward extension of stratospheric northern annular mode anomalies. *Climate Dyn.*, **55**, 595–612, https://doi.org/10.1007/s00382-020-05285-4.

Zhao, B., B. Zhang, C. X. Shi, J. W. Liu, and L. P. Jiang, 2019: Comparison of the global energy cycle between Chinese Reanalysis Interim and ECMWF reanalysis. *Journal of Meteorological Research*, **33**, 563–575, https://doi.org/10.1007/s13351-019-8129-7.

Zhao, D., L. X. Zhang, T. J. Zhou, and J. W. Liu, 2021: Contributions of local and remote atmospheric moisture fluxes to east China precipitation estimated from CRA-40 reanalysis. *Journal of Meteorological Research*, **35**, 32–45, https://doi.org/10.1007/s13351-021-0083-5.

Zheng, Y. Q., S. F. Chen, W. Chen, and B. Yu, 2021: Diverse influences of spring Arctic Oscillation on the following winter El Niño–Southern Oscillation in CMIP5 models. *Climate Dyn.*, **56**, 275–297, https://doi.org/10.1007/s00382-020-05483-0.